



HAL
open science

An ancient divide in outer membrane tethering systems in bacteria suggests a mechanism for the diderm-to-monoderm transition

Jerzy Witwinowski, Anna Sartori-Rupp, Najwa Taib, Nika Pende, To Nam
Tham, Daniel Poppleton, Jean-Marc Ghigo, Christophe Beloin, Simonetta
Gribaldo

► To cite this version:

Jerzy Witwinowski, Anna Sartori-Rupp, Najwa Taib, Nika Pende, To Nam Tham, et al.. An ancient divide in outer membrane tethering systems in bacteria suggests a mechanism for the diderm-to-monoderm transition. *Nature Microbiology*, 2022, 7 (3), pp.411-422. 10.1038/s41564-022-01066-3 . pasteur-03682191

HAL Id: pasteur-03682191

<https://pasteur.hal.science/pasteur-03682191>

Submitted on 2 Jun 2022

HAL is a multi-disciplinary open access archive for the deposit and dissemination of scientific research documents, whether they are published or not. The documents may come from teaching and research institutions in France or abroad, or from public or private research centers.

L'archive ouverte pluridisciplinaire **HAL**, est destinée au dépôt et à la diffusion de documents scientifiques de niveau recherche, publiés ou non, émanant des établissements d'enseignement et de recherche français ou étrangers, des laboratoires publics ou privés.



Distributed under a Creative Commons Attribution - NonCommercial 4.0 International License

1 **An ancient divide in outer membrane tethering systems in Bacteria suggests a**
2 **possible mechanism for the diderm-to-monoderm transition**

3

4 Jerzy WITWINOWSKI¹, Anna SARTORI-RUPP^{3,+}, Najwa TAIB^{1,4,+}, Nika PENDE¹, To
5 Nam THAM¹, Daniel POPPLETON^{1,5}, Jean-Marc GHIGO², Christophe BELOIN^{2*},
6 Simonetta GRIBALDO^{1*}

7

8 ¹ Institut Pasteur, Université de Paris, UMR CNRS2001, Unit Evolutionary Biology of
9 the Microbial Cell, 75015 Paris, France

10 ² Institut Pasteur, Université de Paris, UMR CNRS2001, Genetics of Biofilms
11 Laboratory, 75015 Paris, France

12 ³ Institut Pasteur, Université de Paris, Unit of Technology and Service Ultra-
13 structural Bio-Imaging, 75015 Paris, France

14 ⁴ Institut Pasteur, Université de Paris, Hub Bioinformatics and Biostatistics, F-75015
15 Paris, France

16 ⁵ Sorbonne Université, Collège doctoral, F-75005 Paris, France

17

18

19 *Corresponding authors:

20 christophe.beloin@pasteur.fr

21 simonetta.gribaldo@pasteur.fr

22

23 ⁺ These authors contributed equally to this work

24

25 **Abstract**

26 Recent data support the hypothesis that Gram-positive bacteria (monoderms) arose
27 from Gram-negatives (diderms) through loss of the outer membrane (OM), but how
28 this happened remains unknown. As tethering of the OM is essential for cell envelope
29 stability in diderm bacteria, its destabilization may have been involved in this
30 transition. Here, we present an in-depth analysis of the four known main OM tethering
31 systems across the Tree of Bacteria (ToB). We show that the presence of such systems
32 follows the ToB with a bimodal distribution matching the deepest phylogenetic
33 divergence between Terrabacteria and Gracilicutes. Whereas the lipoprotein Pal is
34 restricted to the Gracilicutes along with a more sporadic occurrence of OmpA, and
35 Braun's lipoprotein Lpp is present only in a subclade of Gammaproteobacteria, diderm
36 Terrabacteria display as the main system the OmpM protein. We propose an
37 evolutionary scenario whereby OmpM represents a simple, ancestral OM tethering
38 system that was later replaced by one based on Pal following the emergence of the Lol
39 machinery to deliver lipoproteins to the OM, with OmpA as a possible transition state.
40 We speculate that the existence of only one main OM tethering system in the
41 Terrabacteria would have allowed the multiple OM losses specifically inferred in this
42 clade through OmpM perturbation, and we provide experimental support for this
43 hypothesis by inactivating all four *ompM* gene copies in the genetically tractable
44 diderm Firmicute *Veillonella parvula*. High-resolution imaging and tomogram
45 reconstructions reveal a non-lethal phenotype in which vast portions of the OM detach
46 from the cells, forming huge vesicles with an inflated periplasm shared by multiple
47 dividing cells. Together, our results highlight an ancient shift of OM tethering systems
48 in bacterial evolution and suggest a possible mechanism for OM loss and the multiple
49 emergences of the monoderm phenotype from diderm ancestors.

50 Introduction

51 The shift between monoderms and diderms is one of the major transitions in the
52 evolution of Bacteria (for two recent reviews see ¹ and ²). Growing evidence that the
53 majority of bacterial phyla are diderms, and that monoderms do not constitute a
54 monophyletic clade suggests that the outer membrane (OM) is an ancestral character
55 that was lost multiple times during evolution ^{1,3,4}. Although the mechanisms are
56 unknown, one of them could have involved destabilization of OM attachment ⁵.

57 In diderm bacteria, tethering of the OM to the cell wall is of fundamental
58 importance to preserve cell envelope integrity. OM tethering has been mostly studied
59 in *Escherichia coli*, where at least three different systems are identified (**Figure 1**). The
60 best known is Braun's lipoprotein (Lpp), which forms a covalent link between the OM
61 and peptidoglycan (PG) ^{6,7}. Lpp mutants present increased sensitivity to membrane
62 stress and higher OM permeability with bleb formation and hypervesiculation in
63 minimal media ⁸⁻¹¹. A second OM tethering system is based on the Pal lipoprotein,
64 which attaches non-covalently both to PG and to the inner membrane protein TolB
65 ^{10,12,13}. Pal mutants display similar, yet more severe defects than Lpp mutants, including
66 problems with OM constriction at the division plane, also considering that this protein
67 plays multiple cellular functions ^{10,11,14-16}. Finally, it was demonstrated that the beta
68 barrel OM protein OmpA, sharing a homologous PG-binding domain with Pal, also
69 plays a role in OM attachment in *E. coli* ^{10,17,18}. In *E. coli* the three systems are at least
70 partially redundant as overexpression of Pal or OmpA suppresses the defects of the
71 *lpp* null mutant^{10,13,17,18}.

72 Recent analyses have shown that the most ancient divide in Bacteria likely
73 occurred between two large clades, the Terrabacteria (which encompass both
74 monoderm and diderm phyla, like Cyanobacteria, Firmicutes, Actinobacteria,

75 Synergistetes, Thermus/Deinococcus, Thermotogae, Chloroflexi, the Candidate Phyla
76 Radiation/CPR) and the Gracilicutes (which include only diderm phyla, such as
77 Proteobacteria, the Planctomycetes/Verrucomicrobia/Chlamydiae superphylum,
78 Bacteroidetes, Spirochaetes)^{1,3,4}. Within Terrabacteria, the Firmicutes (low GC Gram-
79 positives) represent an ideal model to study the diderm to monoderm transition: they
80 comprise in fact at least three independent clades that display an OM with
81 lipopolysaccharide: the *Negativicutes*, the *Halanaerobiales* and the *Limnochordia*^{1,3,19,20}.
82 We have recently proposed that the OM is an ancestral character of all Firmicutes and
83 was lost repeatedly during their diversification, giving rise to the classical monoderm
84 cell envelope in this phylum^{1,3,20}. Diderm Firmicutes lack homologues of Lpp and Pal,
85 but instead possess a fourth type of OM attachment (**Figure 1**). It was first
86 characterized by *in vitro* analysis of a recombinant protein from the Negativicute
87 *Selenomonas ruminantium*, originally named Mep45 (Major Envelope Protein of 45 kDa)
88 and later OmpM²¹⁻²⁴. OmpM is composed of a beta barrel that inserts into the OM and
89 an N-terminal S-Layer Homology (SLH) domain that binds *in vitro* to PG modified
90 with aliphatic polyamines such as cadaverine or putrescine^{23,25,26}. OmpM homologues
91 are present in all diderm Firmicute genomes, frequently in multiple copies and often
92 displaying a conserved genomic context together with other proteins related to OM
93 biogenesis and maintenance^{1,3,20}. The first proteomic characterization of the OM in the
94 Negativicute *Veillonella parvula* DSM2008 showed that two of its four OmpM proteins
95 are among the most abundant OM components²⁷.

96 Interestingly, OmpM proteins seem to be present in other diderm phyla within
97 the Terrabacteria. In *Synechococcus* (Cyanobacteria), it was shown that proteins
98 composed of a periplasmic SLH domain and an OM beta-barrel (an architecture, which
99 defines OmpM) attach the OM to the PG and their depletion leads to OM stability

100 defects ^{28,29}. Similarly, a protein bearing the same architecture, named Slp, was
101 identified in *Thermus thermophilus* (Deinococcus/Thermus), and shown to be involved
102 in the attachment of the outer layer of the cell envelope, although not described at the
103 time as a *bona fide* OM ^{30,31}. However, cadaverination of PG does not seem to be
104 involved in either of these bacteria, instead the SLH domain of OmpM recognizes
105 pyruvylated secondary cell wall polymers, and deletion of the pyruvyl transferase
106 responsible for this modification (CsaB) led to the same phenotype as
107 deletion/depletion of the OmpM homolog ^{29,32}. Finally, two proteins, Omp α and
108 Omp β , were identified as major OM components in the Thermotogae, each
109 corresponding to the SLH and porin domains, respectively, but lack of genetic tools
110 has prevented the construction and analysis of mutants ³³.

111 The existence of four main OM tethering systems in Bacteria poses the question
112 of when they originated and how they evolved. To this aim, we explored their
113 occurrence and evolution across all Bacteria, and we complemented this analysis by
114 experimental inactivation of OmpM in *V. parvula*. Together, our results highlight a
115 major and ancient divide in the way bacteria tether their OM, and allow us to discuss
116 the hypothesis that perturbation of OmpM-based OM tethering was a possible
117 mechanism for the repeated OM losses and transitions to the monoderm phenotype,
118 which occurred specifically in the Terrabacteria. We propose diderm Firmicutes as
119 ideal models to understand the mechanisms involved in OM stability and
120 maintenance, opening the way to replay the monoderm/diderm transition in the
121 laboratory.

122

123 Results

124 OM tethering systems display a bimodal distribution

125 We carried out an in-depth analysis of the four main OM attachment systems
126 (OmpM, Lpp, Pal, OmpA) across 1093 genomes representing all current bacterial
127 diversity and mapped them onto a reference phylogeny of Bacteria (Supplementary
128 Data Sheet 1A and Figure 2). Strikingly, we could identify OmpM homologues in all
129 diderm Terrabacteria phyla, including diderm Firmicutes (**Figure 2a**, light blue dots),
130 but never in the Gracilicutes.

131 In agreement with the experimental characterizations mentioned above, we
132 detected OmpM homologues in *Deinococcus/Thermus*, as well as in Cyanobacteria
133 and their uncultured sister clades (Figure 2a). Cyanobacteria have two paralogues of
134 OmpM, which were differently retained across species (Supplementary Figure S1a and
135 Supplementary Results and Discussion 1.1). We identified Omp α and Omp β in all
136 Thermotogae and their neighbor candidate phyla Bipolaricaulota and Fraserbacteria
137 (**Figure 2**, darker blue dots), and phylogenetic analysis suggests that they are *bona fide*
138 homologues of canonical OmpM (Supplementary Figure S1 and Supplementary
139 Results and Discussion 1.2). Finally, multiple copies of OmpM are often present in the
140 *Negativicutes* (Extended Data Figure ED1, Supplementary Data Sheet 1C, and
141 Supplementary Results and Discussion 1.3).

142 In contrast, Pal homologues display a distribution complementary to OmpM,
143 being largely present in the Gracilicutes, while they are totally absent from the
144 Terrabacteria (**Figure 2**, green dots). The distribution of OmpA is patchier (**Figure 2**,
145 dark violet dots), but it also concentrates mainly in the Gracilicutes. Within
146 Terrabacteria, we could only find OmpA homologues in some *Negativicutes* (including
147 *V. parvula*), and in two candidate phyla (Margulisbacteria and

148 Wallbacteria/Rifl bacteria), which were likely acquired via horizontal gene transfers
149 from the Gracilicutes (Supplementary Figure S1b). Finally, whereas Lpp is largely
150 considered as the textbook example of OM tethering, it is in fact restricted to a subclade
151 of *Gammaproteobacteria* (orders *Aeromonadales*, *Alteromonadales*, *Enterobacterales*, and
152 *Vibrionales*) (**Figure 2** and Supplementary Data Sheet 1E), extending recent analyses on
153 a much smaller taxonomic sampling^{34,35}.

154 These results highlight the existence of a major divide in how diderm bacteria
155 attach their OM, OmpM and Pal representing the main mechanisms in Terrabacteria
156 and Gracilicutes, respectively. Because Pal is a lipoprotein, its origin may be linked
157 with the emergence of the Lol system, the machinery delivering lipoproteins to the
158 OM³⁶. Indeed, while the Lol system is widely distributed in the Gracilicutes, and
159 notably every time that Pal is present (**Figure 2**, orange dots, and Supplementary Data
160 Sheet 1A and B), we could not find any homologues of the components of the Lol
161 machinery in the Terrabacteria, with the exception of *Deinococcus/Thermus* (likely
162 acquired by horizontal gene transfer, Supplementary Figure S2).

163 Finally, because the few characterized OmpM-based tethers seem to all use
164 recognition between the SLH domain and pyruvylated secondary cell wall polymers
165 (the use of cadaverinated PG in the *Negativicutes* possibly being an exception, see
166 Supplementary Results and Discussion 1.4), we analyzed the distribution of
167 homologues of CsaB, the pyruvyl transferase that is responsible for the PG
168 modification, and of the SLH domains (Supplementary Data Sheet 1D). Indeed, CsaB
169 and SLH co-occur in most diderm Terrabacteria (**Figure 2**, lilac dots), extending what
170 previously noticed on a smaller taxonomic sample³⁷, and match closely the
171 distribution of OmpM, but are instead practically absent in the Gracilicutes. This

172 correlation strongly suggests that OM attachment to pyruvylated PG is a conserved
173 feature of diderm Terrabacteria.

174

175 **Deletion of OmpM in *V. parvula* leads to a striking phenotype**

176 The presence of one major OM tethering system in the Terrabacteria may explain why
177 there were multiple independent losses of the OM specifically in this clade (**Figure 2**).

178 We therefore sought to investigate the consequences of perturbing OM attachment by
179 deleting OmpM in the genetically tractable diderm Firmicute *Veillonella parvula*. The
180 *V. parvula* SKV38 genome contains four OmpM coding genes, as well as a predicted
181 gene coding for an OmpA homologue, but no Lpp or Pal homologues. We constructed
182 a mutant of the three adjacent *ompM1* to *ompM3* genes ($\Delta ompM1-3$), a mutant of the
183 *ompM4* gene ($\Delta ompM4$), which lies elsewhere in the genome, a quadruple deletion
184 mutant ($\Delta ompM1-4$), a mutant of *ompA* ($\Delta ompA$) and a quintuple mutant
185 ($\Delta ompA\Delta ompM1-4$). We could not obtain single gene mutants of the *ompM1-3* genes
186 due to their very similar nucleotide sequences (Supplementary Figure S3), and the fact
187 that the intergenic regions are equally similar.

188 With respect to the wild type, the $\Delta ompM1-3$ and $\Delta ompM1-4$ strains presented
189 severe growth defects, and were extremely sensitive to sodium deoxycholate, EDTA,
190 SDS, and vancomycin (**Figure 3a**, Extended Data Table ED1). On the contrary, the
191 $\Delta ompM4$ and $\Delta ompA$ mutants were not affected (**Figure 3a**, Extended Data Table ED1).
192 The quintuple $\Delta ompA\Delta ompM1-4$ mutant had the strongest growth defect and
193 sensitivity to stress (**Figure 3a**, Extended Data Table ED1). This may be linked to the
194 fact that it lacks five of the six porins predicted in the genome (the sixth being
195 FNLLGLLA_00833, not involved in OM attachment as it has no PG attachment

196 domain) likely impairing the uptake of nutrients and exchanges with the environment
197 rather than cell envelope organization.

198 Under light microscopy, the $\Delta ompM1-3$ mutants displayed very large vesicles,
199 with sizes ranging from a few hundred nanometers to $\sim 8 \mu\text{m}$ in diameter (**Figure 3b**).
200 The quadruple ($\Delta ompM1-4$) and quintuple ($\Delta ompA\Delta ompM1-4$) mutants presented a
201 phenotype similar to $\Delta ompM1-3$, whereas the $\Delta ompM4$ and $\Delta ompA$ mutants were not
202 affected in cell morphology (**Figure 3b**). Finally, expression *in trans* of both native and
203 HA-tagged *ompM1*, whose homologue in *V. parvula* DSM2008 corresponds to the most
204 abundant outer membrane protein ²⁷, almost completely reverted the mutant
205 phenotype (Extended Data Table ED1, Extended Data Figure ED2). However, this was
206 not the case of native or HA-tagged variants of the *ompA* and *ompM4* genes (Extended
207 Data Figure ED3). OmpM4 displays indeed specific differences in its SLH domain with
208 respect to OmpM1-3 proteins that may make it nonfunctional or less efficient
209 (Supplementary Figure S4 and Supplementary Results and Discussion 2).

210 Altogether, these results suggest that OmpM1-3 represent the main system
211 responsible for OM tethering in *V. parvula*, and that OmpA and OmpM4 have a less
212 important role, or even a different one, such as the exchange of nutrients or /and toxic
213 metabolic products with the environment via their porin component. We therefore
214 focused on further analysis of the triple $\Delta ompM1-3$ mutant.

215

216 **Ultrastructural details of the *V. parvula* $\Delta ompM1-3$ mutant**

217 High-resolution 3D Structured Illumination Microscopy (3D SIM) of the
218 $\Delta ompM1-3$ mutant revealed further its defects as compared to the WT (Figure 4). In the
219 mutant, the OM appeared substantially detached and formed very large vesicular
220 structures, within which cells appeared to continue dividing as shown by the presence

221 of multiple nucleoids (**Figure 4b** and **4c**). In contrast, the mutants complemented by
222 expression of OmpM1 had a phenotype undistinguishable from the WT (**Figure 4a** and
223 **4d**), whereas this was not the case in the absence of induction (**Figure 4e**). Finally, some
224 vesicles appeared empty as devoid of any DNA signal (**Figure 4b**, white arrows and
225 the inlet in **Figure 4e**).

226 Although the thickness of the frozen samples (~400-500 nm) was at the limit of
227 observable objects by Cryo-ET, we obtained additional insights into the ultrastructural
228 organization of the $\Delta ompM1-3$ mutant with respect to the WT (**Figure 5a-c**, Extended
229 Data Figure ED4, Supplementary Movies S1-3). *V. parvula* WT cells are cocci with a
230 perfectly visible diderm envelope (**Figure 5a**). In the $\Delta ompM1-3$ mutant, the cells
231 conserved their coccus shape, and were surrounded by the IM and a contiguous layer
232 of slightly but significantly thicker PG (15.7 ± 2.4 nm (n=30) as compared to $11.7 \pm$
233 1.8 nm (n=30) in the WT; $p < 10^{-5}$ according to two-tailed Student's t test and
234 permutation test for independent groups). However, the OM appeared vastly
235 detached from the cell body, forming an enlarged, inflated periplasm with a higher
236 density than the surrounding medium (suggesting the presence of normal
237 proteinaceous periplasmic components), shared by numerous dividing cells (**Figure**
238 **5b** and **5c**, Extended Data Figure ED4, Supplementary Movies S2 and S3). The inner
239 diameter of the cells was 549 ± 46 nm (n=37), not significantly different from the WT
240 (560 ± 37 nm (n=37)) according to two-tailed Student's test and permutation test for
241 independent groups. Consistent with the 3D-SIM images, cells within the vesicles
242 displayed partial attachment to the OM, possibly helped by the presence of envelope-
243 spanning machineries (see also Supplementary Results and Discussion 3). In some
244 cases, the vesicles also contained degraded cells with patches of IM still attached to the
245 OM (**Figure 5b**, yellow asterisk). Most of the large vesicles were connected by pearling

246 OM tubes that could reach a few tenths of microns in length, probably remnants of
247 budding vesicles (**Figure 5b**, white arrows). In some of the samples embedded in
248 thinner ice, even surface pili or fimbriae still linked to the detached OM could be
249 visualized (**Figure 5b** and Extended Data Figure ED4, pink arrows). Strikingly, the
250 strong phenotype of the $\Delta ompM1-3$ could be totally rescued by *in trans* expression of
251 *ompM1*, indicating that a single OmpM manages to restore OM tethering (**Figure 5d**,
252 Supplementary Movie S4).

253

254 Discussion

255 Our results reveal an ancient divide in the systems involved in OM stability in
256 Bacteria and suggest a plausible scenario for their origin and evolution. Current
257 evidence points to a common ancestor of all Bacteria that already possessed a complex
258 diderm cell envelope^{1,3,4}. This implies that it would have needed an OM tether. Our
259 results suggest that Pal and Lpp emerged within the Gracilicutes, whereas OmpM and
260 OmpA appear to be the most ancient OM tethers, being present in deep branches of
261 the Terrabacteria and Gracilicutes, respectively (**Figure 2**). Two possible scenarios can
262 be put forward for the origin and evolution of OmpM and OmpA (**Figure 6**). In the
263 first scenario, OmpM would represent a simple system that was already present in the
264 Last Bacterial Common Ancestor (LBCA) (**Figure 6**, scenario 1) allowing OM tethering
265 while at the same time fulfilling a generalist porin function of diffusion through the
266 membrane, as shown experimentally for the OmpM of the Negativicute *S. ruminantium*
267³⁸ and for Slp of *D. radiodurans*³⁹. This ancestral OmpM system would have been
268 inherited in the branch leading to present day Terrabacteria and replaced in the branch
269 leading to Gracilicutes by OmpA, followed by the progressive appearance of the other
270 multiple redundant systems (Pal, Lpp). OmpA may represent a possible transition

271 state in this scenario, as it is the only system present in Fusobacteria and Spirochaetes,
272 two phyla at the interface between Terrabacteria and Gracilicutes (**Figure 2**). OmpA
273 would have replaced OmpM by still being able to use its integral OM beta barrel to
274 attach to the OM but switching its PG attachment from the SLH domain to an OmpA
275 domain. This change in interaction would have made dispensable in the Gracilicutes
276 the specific PG modifications (secondary cell wall polymers or cadaverine) needed for
277 SLH domain binding by OmpM in diderm Terrabacteria. An alternative scenario
278 (**Figure 6**, scenario 2) would place OmpA as the ancestral OM tethering system in the
279 LCBA. In this case, OmpA would have been replaced by an OmpM-based system in
280 the lineage leading to Terrabacteria following the appearance of pyruvylation of
281 secondary cell wall polymers by CsaB and of SLH domains capable of recognizing it.
282 As an alternative to these two scenarios, it cannot be excluded that both OmpM and
283 OmpA were ancestrally present and were later independently lost in the lineage
284 leading to the Gracilicutes or the Terrabacteria, respectively, or even that the LBCA
285 had a completely different type of OM tether.

286 In all scenarios, the appearance of multiple OM tethering systems in the
287 Gracilicutes would have followed the same path (**Figure 6**). It is likely that Pal
288 originated from OmpA, as suggested by the fact that they share the same domain to
289 attach to PG and differ only by the mechanism of attachment to the OM. To be inserted
290 correctly into the OM, Pal needs the Lol machinery and could have therefore only have
291 appeared after – or in concomitance with – the emergence of this system. It may be
292 argued that OM lipoproteins were already present in the LBCA and were exported
293 and inserted by another, yet unknown mechanism, which would have been inherited
294 in the Terrabacteria but replaced by Lol in the Gracilicutes. However, a few arguments
295 weaken this hypothesis. There is currently no experimental evidence for the presence

296 of OM lipoproteins in members of the Terrabacteria, to the exception of
297 *Deinococcus/Thermus*, which in fact acquired a Lol system secondarily via horizontal
298 gene transfer from the Gracilicutes (Supplementary Figure S2). The report of OM
299 lipoproteins in Cyanobacteria⁴⁰ is unclear, as admitted by the authors, because all the
300 lipoproteins found in the OM preparations were also found in the IM preparations,
301 and all but one also in the thylakoid membrane preparations. In addition, the study of
302 the *V. parvula* proteome found the presence of lipoproteins in the IM but not the OM
303 ²⁷. Finally, the absence of OM lipoproteins in the Terrabacteria would also be consistent
304 with the fact that the major machineries for OM biosynthesis such as Bam and Lpt lack
305 specifically in this clade the OM lipoprotein components found in the Gracilicutes (⁴¹⁻
306 ⁴³ and personal observations).

307 The reasons for takeover of OM tethering by multiple redundant systems in the
308 Gracilicutes are unclear. The apparent much larger diversification of the Gracilicutes
309 with respect to the Terrabacteria (**Figure 2**) suggests that this may have been
310 advantageous, for instance by providing a stronger attachment allowing higher
311 resistance to stress on the OM. This tight tethering could be the reason why no loss of
312 the OM ever occurred in the Gracilicutes. It is true that not all Gracilicutes have
313 redundant systems, with some members appearing to possess only Pal (**Figure 2**). It is
314 possible that Pal provides alone a strong tether in these species, but also it is not
315 excluded that they have additional alternative systems. Indeed, two completely novel
316 OM attachment systems have been recently described in Proteobacteria involving
317 porins⁴⁴⁻⁴⁶: a two component system in which a periplasmic protein PapA attaches both
318 to the peptidoglycan and to the integral outer membrane beta barrel protein OmpC,
319 common in *Betaproteobacteria*⁴⁶, and numerous beta barrel outer membrane proteins

320 covalently attached to the peptidoglycan in *Alphaproteobacteria* but also in some
321 *Gammaproteobacteria*^{44,45}.

322 The situation is strikingly different in the Terrabacteria, which show more
323 variability of cell envelopes, and where multiple independent losses of the OM can be
324 inferred, at least at the divergence of three large clades of monoderms (Actinobacteria,
325 Chloroflexi, and CPR), and multiple times within the Firmicutes (**Figure 2**). It is
326 tempting to speculate that these multiple OM losses are linked to the presence of only
327 a single main OM attachment represented by OmpM, which could have made
328 members of Terrabacteria somehow more permissive to cell envelope perturbation.
329 The state observed in Thermotogae, where the OM is largely detached at the cell
330 poles³³, as well as the rotund bodies (where one OM surrounds multiple cells)
331 observed in Dictyoglomi and Deinococcus/Thermus^{47,48} might testify to such higher
332 instability.

333 We propose that inactivation of OmpM may have been one the evolutionary
334 mechanisms for loss of the OM and the emergence of monoderms from diderms. The
335 mechanistic details of this transition are currently unclear. Increase in PG thickness to
336 compensate for OM instability may have been an important step, similarly to what we
337 observed in our *V. parvula* $\Delta ompM1-3$ mutant. Whether this increase is a mechanical
338 consequence of the space left by a larger periplasm and/or a reaction to cell envelope
339 stress caused by OM detachment remains to be determined. It may be also wondered
340 if vestiges of the OmpM system were maintained after OM loss. From our analysis it
341 appears that transition to the monoderm cell envelope was often accompanied not only
342 by loss of the porins but also the SLH domains, together with the CsaB enzyme
343 allowing the PG modification necessary for their attachment (**Figure 2**). In some
344 monoderm lineages, the SLH/CsaB system was kept and possibly repurposed for

345 other functions. Functional repurposing is clearly visible in the Firmicutes, where the
346 SLH/CsaB system was largely kept, despite the multiple losses of the OM (see
347 Supplementary Results and Discussion 5).

348 Our results clearly demonstrate that OmpM and Pal can be considered as
349 markers of either diderm Terrabacteria or Gracilicutes, respectively. As such, their
350 presence in newly reconstructed genomes from uncultured bacterial lineages may
351 facilitate their taxonomic assignment. Moreover, their presence/absence may be used
352 to infer a diderm or monoderm phenotype in the vast majority of phyla for which cell
353 envelope characterization is missing. For example, the absence of OmpM from the
354 Chloroflexi favors the hypothesis that the diderm-like envelopes recently observed in
355 members of this phylum may actually be other types of structures ⁴⁹.

356 The lack of any predicted OM attachment system in some diderm genomes
357 (**Figure 2**) is intriguing. While this can be explained by genome incompleteness in
358 uncultured candidate phyla, the specific case of Planctomycetes is particularly
359 interesting. Members of this phylum have an atypical diderm cell envelope and for a
360 long time were believed to lack peptidoglycan ⁵⁰. Their cell membrane is also unusually
361 dynamic, thanks to the presence of membrane coat proteins of eukaryotic type ⁵¹. It is
362 possible that due to these particularities, they either evolved a novel attachment
363 system, or modified so profoundly the one inherited from their ancestor that it cannot
364 be recognized anymore.

365 Finally, our study highlights the genetically amenable diderm Firmicutes *V.*
366 *parvula* as an ideal new experimental model with respect to more classical Gracilicutes
367 models such as *E. coli*, which have an arsenal of – mostly non-essential – tethering
368 systems and where no similarly dramatic phenotypes arising from OM perturbation
369 have been observed. Further study of *V. parvula* will therefore allow a better

370 understanding of the multiple processes involved in the biogenesis of the diderm cell
371 envelope, and the mechanisms employed for maintaining OM integrity, an area of
372 intense interest in the fight of bacterial pathogens. Finally, the *V. parvula* OM
373 attachment mutant described in this work opens the way to further experimental work
374 that may allow to recapitulate and study the diderm-to-monoderm transition in the
375 laboratory.

376

377 **Methods**

378

379 Sequence analysis

380 We assembled a databank of 1,093 genomes representing all bacterial phyla
381 present at the National Center for Biotechnology (NCBI) as of April 2020. We selected
382 three species per order for each phylum. The number of genomes per phylum therefore
383 reflects their taxonomical diversity (for a list of taxa see Supplementary Data Sheet 1).
384 We chose preferably genomes from reference species and the most complete
385 assemblies. We then queried this databank for the presence of Lpp, Pal, OmpA,
386 OmpM, as well as for the Lol system and CsaB homologues. Total absences of a given
387 homologue in a phylum was confirmed by checking all the genomes available in the
388 NCBI.

389 To identify Lpp and CsaB homologues, we used HMMSEARCH from the
390 HMMER 3.3.2 package ⁵², and screened the databank using the Pfam domains LPP
391 (PF04728) and PS_pyruv_trans (PF04230) with the option --cut_ga, the gathering
392 threshold assigned by curators and corresponding to the minimum score a sequence
393 must attain in order to belong to the full alignment of a Pfam entry. We also searched
394 for Lpp homologues in a specific databank of 1083 Proteobacteria including
395 genomes from *Gammaproteobacteria*.

396 For the Lol system, we started by searching LolA in the databank using the Pfam
397 domain PF03548 and HMMSEARCH with the option --cut_ga. As it is known that in
398 some taxa LolA might be absent while the other components are present, we also
399 searched for the ABC transporters LolC, LolD and LolE in a reduced databank
400 composed of genomes from 192 taxa representing 36 main bacterial phyla. The
401 alignments of protein families PRK10814 (LolC), PRK11629 (LolD) and PRK11146

402 (LolE) were downloaded from NCBI (Conserved Domain Database). HMM profiles
403 were build using HMMBUILD from the HMMER 3.3.2 package and used to query the
404 reduced databank. Because ABC transporter subunits belong to large protein families,
405 the results were curated manually using annotations, synteny, alignments and
406 phylogeny. Results were pooled for the LolC/E components, as search outputs
407 overlapped greatly, and only a clade within *Gammaproteobacteria* possessed these
408 distinct two paralogs.

409 As OmpA and Pal homologues share the same OmpA domain (PF00691), a
410 specific strategy was applied to distinguish them: we first searched for proteins
411 containing the OmpA domain using HMMSEARCH and the --cut_ga option; the
412 retrieved hits were then submitted to PRED-TMBB 2 analysis ⁵³ to select those
413 containing a beta barrel, and the positive matches were considered as OmpA proteins.
414 As PRED-TMBB 2 generates many false positives, in case of doubt the presence of a
415 beta barrel was confirmed or invalidated with BOCTOPUS2 ⁵⁴. OmpA homologues
416 were also identified in the same way in a local database of 230 Firmicutes. To identify
417 Pal homologues, we used MacSyFinder 1.0.5 ⁵⁵ to investigate the immediate genetic
418 context of OmpA-containing proteins for the presence of a TolB homologue using the
419 Pfam domains TolB_N (PF04052), TolB_like (PF15869), WD40 (PF00400) and PD40
420 (PF07676).

421 OmpM were defined as proteins containing an SLH domain and a beta barrel
422 porin. To find OmpM homologues, we therefore first screened our genome databank
423 for the presence of proteins containing SLH domains (PF00395) with HMMSEARCH
424 and the --cut_ga option. All the hits also containing a beta barrel were then identified
425 by using PRED-TMBB 2 and BOCTOPUS2. In Thermotogae, Bipolaricaulota and
426 Fraserbacteria, the SLH domain and the beta barrel are split into two adjacent proteins.

427 To detect this configuration, we screened the proteins with an SLH domain for the
428 presence of neighboring beta barrel structures. Results were manually curated using
429 alignment, functional annotation, protein domains and phylogeny.

430 Finally, the presence/absence of each OM attachment system was mapped onto
431 a reference tree of Bacteria using custom made scripts and iTOL ⁵⁶.

432

433 Phylogenetic analysis

434 To build the reference bacterial phylogeny, we assembled a smaller database of
435 377 genomes by selecting five taxa per phylum. We selected 15 representatives from
436 the CPR and 46 from the Proteobacteria, as they are very diverse. Hidden Markov
437 model (HMM)-based homology searches (with the option --cut_ga) were carried out
438 with HMMSEARCH by using the pfam profiles PF04997.12, PF04998.17, PF04563.15,
439 PF00562.28 and PF11987.8 corresponding to RNA polymerase subunits β , β' and
440 translation initiation factor IF-2. Single genes were aligned using MAFFT v7.407 with
441 the L-INS-I option, and trimmed using BMGE-1.12 ⁵⁷ with the BLOSUM30 substitution
442 matrix. The resulting trimmed alignments were concatenated into a supermatrix (377
443 taxa and 2,206 amino acid positions). The ML tree was generated using IQ-TREE v.1.6.3
444 with the profile mixture model LG+C60+F+G, with ultrafast bootstrap supports
445 calculated on 1,000 replicates of the original dataset. Curated OmpA homologues were
446 aligned using MAFFT v7.407 with the L-INS-I option and the alignment trimmed with
447 trimal with the option -gt 0.5. The tree was built using IQ-TREE with the best-fit model
448 LG+F+G4 estimated by ModelFinder, and ultrafast bootstrap supports computed on
449 1000 replicates of the original dataset.

450 For the lol system analysis, curated LolD homologues were aligned using
451 MAFFT v7.407 with the L-INS-I option and the alignment trimmed with BMGE-1.12

452 using BLOSUM30 replacement matrix. The tree was built using IQ-TREE with the best-
453 fit model LG+G4+I+F estimated by ModelFinder, and ultrafast bootstrap supports
454 computed on 1000 replicates of the original dataset. The same procedure was applied
455 for curated LolCE homologues.

456 For the detailed analysis of the distribution of OmpM in the *Negativicutes*, we
457 assembled a local database of 135 *Negativicute* proteomes, and we applied the same
458 strategy as outlined above. Results were plotted onto a reference phylogenetic tree of
459 *Negativicutes* based on a concatenation of translation initiation factor IF-2, and RNA
460 polymerase subunits β and β' assembled as above. Sequences were aligned using
461 MAFFT v7.407, trimmed using BMGE-1.12, concatenated (3027 amino acid positions
462 per sequence in final alignment) and the tree was generated using IQ-TREE with the
463 best fit LG+R5 model estimated by ModelFinder.

464 For the detailed analysis of the distribution of SLH domains and CsaB proteins
465 in Firmicutes a local database of 230 Firmicutes was queried with HMMER 3.3.2
466 package using the HMM profiles for SLH (PF00395) and PS_pyruv_trans (PF04230)
467 domains downloaded from pfam.xfam.org using the `-cut_ga` option.

468 Curated OmpM homologues (for OmpM-like proteins, we concatenated Omp α
469 and Omp β sequences) were aligned using MAFFT v7.407⁵⁸ with the L-INS-I option
470 and the alignment was trimmed by using trimal 1.4.22⁵⁹ with the option `-gt 0.7`. The
471 tree was built using IQ-TREE^{60,61} with the best-fit model LG+F+R7 estimated by
472 ModelFinder⁶¹ according to the Bayesian information Criterion (BIC), and ultrafast
473 bootstrap supports⁶² computed on 1000 replicates of the original dataset.

474

475 Bacterial strains, culture conditions and strain manipulation

476 Bacterial strains used in this work are listed in Supplementary Table S1.
477 *Escherichia coli* strains were genetically manipulated using standard laboratory
478 procedures⁶³. When needed, the following compounds were added to *E. coli* cultures
479 at the following concentrations: ampicillin (liquid media) or ticarcillin (solid media) –
480 100 mg/l, chloramphenicol – 30 mg/l (liquid media) or 25 mg/l (solid media),
481 apramycin – 50 mg/l, diaminopimelic acid – 300 μ M, anhydrotetracycline – 250 μ g/l.
482 *V. parvula* was manipulated as described previously^{64,65}, the culture media being
483 either BHILC⁶⁵ or SK⁶⁴. When needed, the following compounds were added to *V.*
484 *parvula* cultures at the following concentrations: chloramphenicol – 25 mg/l,
485 tetracycline – 9 mg/l, erythromycin – 200 mg/l, anhydrotetracycline – 250 μ g/l. The
486 anaerobic conditions were generated using the GenBag Anaer generator (Biomérieux),
487 the C400M anaerobic chamber (Ruskinn) or the GP Campus anaerobic chamber
488 (Jacomex). The anaerobic chambers were filled with a H₂/CO₂/N₂ (5%/5%/90%)
489 mixture.

490

491 Plasmids, primers, and DNA manipulations

492 All plasmids and primers used in this study are listed in Supplementary Table
493 S2 and S3, respectively. Clonings were performed using NEBuilder HiFi DNA
494 Assembly Master Mix (New England Biolabs). Chemocompetent homemade *E. coli*
495 DH5 α cells⁶⁶ were used for transformation of cloning products or plasmids. *V. parvula*
496 genomic DNA was extracted according to a protocol previously described for
497 *Streptomyces* gDNA extraction⁶⁷ from stationary phase cultures in SK medium.

498

499 Conjugation between *E. coli* and *V. parvula*

500 We successfully developed a protocol for conjugative transfer of plasmids from
501 *E. coli* to *V. parvula*, an important addition to the genetic toolbox to manipulate this
502 bacterium. This was especially important when manipulating mutants that have lost
503 their natural competence such as the $\Delta ompM1-3$ strain. The plasmid to conjugate was
504 introduced into *E. coli* MFDpir strain by electrotransformation using standard protocol
505 ⁶⁸. An overnight stationary culture was used to start a fresh culture by 1/100 dilution
506 (180 rpm, 37°C, LB medium). When the culture reached OD₆₀₀ comprised between 0.4
507 and 0.9, the cells were washed twice by an equal volume of LB, resuspended in 1/10
508 of initial volume and stored on ice upon further use. *V. parvula* cultures were launched
509 from cells scratched from a SK petri dish in SK liquid medium at initial OD₆₀₀ of 0.03
510 and grown anaerobically at 37°C until the OD reached 0.1 – 0.2. 0.5 ml of donor *E. coli*
511 strain was mixed with 1 ml of acceptor *V. parvula* strain, centrifugated briefly, the
512 excess volume of medium removed, and the resuspended cells were deposited in form
513 of a droplet on an SK medium plate containing diaminopimelic acid. After 24h of
514 anaerobic incubation at 37°C, the cells were scratched from the Petri dish, resuspended
515 in SK medium and plated on selective SK medium without diaminopimelate.

516

517 Generation of *ompM* and *ompA* deletion mutants

518 The mutants were generated using the technique described previously ⁶⁴.
519 Briefly, for *ompM4* and *ompA* deletion upstream and downstream fragments (about 1
520 kb in size) of the genes to delete as well as the chloramphenicol resistance cassette *catP*
521 were amplified and assembled into one linear construct by PCR. For *ompM1-3* deletion,
522 the tetracycline resistance cassette *tetM* was used. Moreover, as PCR assembly step
523 proved difficult, the three fragments were cloned into the pUC18 *XbaI* site, and then
524 the linear construct was obtained by PCR amplification. Natural competence allowed

525 to transform the SKV38 WT strain with the linear construct and induce homologous
526 recombination (and subsequent gene replacement with the resistance marker), and the
527 correct mutant construction was verified by PCR amplification (and sequencing of
528 amplicons) of the recombination junction zones. The details of the constructions are
529 given in Supplementary Information.

530

531 Generation of quadruple and quintuple mutants

532 To generate a quadruple $\Delta ompM1-4$ mutant, the $\Delta ompM4$ mutant was
533 transformed with $\Delta ompM1-3$ gDNA according to previously established protocol ⁶⁴.
534 The correctness of the mutant was verified by the PCR of the recombination junction
535 zones, and by PCR verification of the absence of *ompM4* gene.

536 To generate a quintuple mutant, a novel linear construct was generated by PCR
537 assembly, using upstream and downstream fragments (slightly below 1 kb in size) of
538 the *ompA* gene, and the *ermE* resistance marker. This construct was used for
539 transformation of the *ompM4* mutant according to previously established protocol ⁶⁴,
540 yielding a $\Delta ompA\Delta ompM4$ strain, which was in turn transformed by the gDNA of the
541 $\Delta ompM1-3$ strain, leading to the desired $\Delta ompA\Delta ompM1-4$ strain. The correct mutant
542 construction was verified by PCR amplification (and sequencing of amplicons) of the
543 recombination junction zones as well as the absence of *ompA* and *ompM4* genes by
544 PCR. The details of the constructions are given in Supplementary Information.

545

546 OmpM1, OmpM4 and OmpA Expression vector construction

547 The expression vectors were constructed by cloning the gene of interest with its
548 native RBS or with a modified RBS into *SacI* site of pRPF185 *Escherichia/Clostridium*
549 conjugative shuttle tetracycline inducible expression vector ⁶⁹. In some vectors, an HA-

550 tag was added during the cloning process into a predicted extracellular loop of the
551 beta barrel (the exact point of insertion of the HA-tag is presented for OmpM1 in the
552 Supplementary Figure S5). The integrity of the constructs was verified by sequencing.
553 The correct expression of HA-tagged protein was verified by Western Blot (Extended
554 Data Figures ED3 and ED5a) and for OmpM1 also by immunomarking (Extended Data
555 Figure ED5b and c). Additionally, the correct expression and addressing to the cell
556 surface was also verified in *E. coli* (Extended Data Figure ED6). All vectors are
557 described in the Supplementary Table S2, and all the details of the construction process
558 are described in Supplementary Information.

559

560 Minimum inhibitory concentration (MIC) determination and growth curves

561 For MIC, serial twofold dilutions of sodium deoxycholate, EDTA, SDS and
562 vancomycin were made in BHILC medium. The dilutions were put in 96-well flat
563 bottom plates (150 μ l per well). Bacterial strains to be tested were grown on SK plates
564 (37°C, anaerobic conditions) for 2-3 days. They were scratched from the plate,
565 resuspended in BHILC medium, and the OD₆₀₀ was adjusted to 1.5. The wells were
566 inoculated with 5 μ l of bacterial suspension to obtain an initial OD₆₀₀ of 0.05 and then
567 incubated anaerobically at 37°C, 180 rpm for 24h. The MIC was defined as the lowest
568 concentration at which the final OD was inferior to 0.1.

569 For growth curves, a 96-well flat bottom plate was filled with 250 μ l per well of
570 BHILC medium. The medium was partially degassed in -0.6 bar vacuum and
571 preincubated 4h inside the GP Campus anaerobic chamber (Jacomex). Then, the wells
572 were anaerobically seeded with 5 μ l of the same bacterial suspension as for the MIC,
573 as the OD in the well was 0.03. The plates were then sealed with Adhesive PCR Plate
574 Seals (Thermo Fisher Scientific). The plates were then incubated in TECAN Sunrise

575 spectrophotometer for 24 hours at 37 °C. OD₆₀₀ was measured every 30 minutes, after
576 15 min of orbital shaking. Each test was performed in pentaplicate.

577

578 Cultures for microscopy observation

579 For *V. parvula*, a liquid culture of 5 ml (in 50 ml Falcon tube) was launched from
580 a glycerol stock in SK medium and incubated anaerobically at 37°C. For strains bearing
581 no plasmid, the observations were made after two days of culture. Like the expression
582 vector bearing strains, at the end of the second day the original culture was diluted
583 10x in fresh medium and incubated anaerobically overnight at 37°C either in presence
584 or absence of anhydrotetracycline.

585 For *E. coli*, a liquid culture of 10 ml (in 50 ml Falcon tube) was launched from a
586 glycerol stock in LB medium and incubated aerobically 24h at 37°C with 180 rpm
587 rotative shaking. A new culture was launched by diluting the original culture 10x in
588 fresh anhydrotetracycline containing medium and then incubated overnight in a 250
589 ml Erlenmeyer flask at 20°C with 180 rpm rotative shaking.

590

591 3D Structured Illumination Microscopy (3D SIM)

592 An aliquot of culture was mixed with FM 4-64 membrane staining dye (Thermo
593 Fischer Scientific) at a final concentration of 5 mg/l and DAPI at a final concentration
594 of 17 mg/l. Bacterial cell suspensions were applied on high precision coverslips (No.
595 1.5H, Sigma-Aldrich) coated with a solution of 0.01 % (w/v) of poly-L-lysine. After
596 letting the cells attach onto the surface of the coverslip for 10 min, residual liquid was
597 removed, 8 µL of antifade mounting medium (Vectashield) were applied and the
598 coverslip was sealed to a slide. SIM was performed on a Zeiss LSM 780 Elyra PS1
599 microscope (Carl Zeiss, Germany) using C Plan-Apochromat 63× / 1.4 oil objective

600 with a 1.518 refractive index oil (Carl Zeiss, Germany). The samples were excited with
601 laser at 405 nm for the DAPI staining and 561 nm for the FM4-64 staining and the
602 emission was detected through emission filter BP 420-480 + LP 750 and BP 570-650 +
603 LP 750, respectively. The fluorescence signal is detected on an EMCCD Andor Ixon
604 887 1 K camera. Raw images are composed of fifteen images per plane per channel
605 (five phases, three angles), and acquired with a Z-distance of 0.10 μm . Acquisition
606 parameters were adapted from one image to one other to optimize the signal to noise
607 ratio. SIM images were processed with ZEN 2012 SP5 FP3 (black) software (Carl Zeiss,
608 Germany) and then corrected for chromatic aberration using 100 nm TetraSpeck
609 microspheres (ThermoFisher Scientific) embedded in the same mounting media as the
610 sample. For further image analysis of SIM image z stacks we used Fiji (ImageJ) Version
611 2.0.0-rc-68/1.52i ⁷⁰. Namely, we assigned a color to the fluorescent channels, stacks
612 were fused to a single image (z projection, maximum intensity) and brightness and
613 contrast were slightly adapted. Regions of interest were cut out and, for uniformity,
614 placed on a black squared background. Figures were compiled using Adobe Illustrator
615 2020 (Adobe Systems Inc. USA).

616

617 Cryogenic electron microscopy observation (CryoEM)

618 A solution of BSA-gold tracer (Aurion) containing 10-nm-diameter colloidal
619 gold particles was added to a fresh culture of *V. parvula* with a final ratio of 3:1. A small
620 amount of the sample was applied to the front (4 μl) and to the back (1.2 μl) of carbon-
621 coated copper grids (Cu 200 mesh Quantifoil R2/2, Quantifoil, or Lacey, EMS),
622 previously glow discharged 2 mA and $1.5\text{-}1.8 \times 10^{-1}$ mbar for 1 min in an ELMO
623 (Corduan) glow discharge system. The sample was then vitrified in a Leica EMGP
624 system. Briefly, the excess liquid was removed by blotting with filter paper the back

625 side of the grids for 6-7 s at 18°C and 95% humidity, and then the sample was rapidly
626 frozen by plunging it in liquid ethane. The grids were stored in liquid nitrogen until
627 image acquisition in the TEM.

628 Cryo-electron microscopy was performed on a Tecnai 20 equipped with a field
629 emission gun and operated at 200 kV (Thermo Fisher) using a Gatan 626 side entry
630 cryoholder. Images were recorded using the SerialEM 3.7 beta software on a Falcon II
631 (FEI, Thermo Fisher) direct electron detector, with a 14 μm pixel size. Digital images
632 were acquired at nominal magnification of 29000x, corresponding to pixel size of 0.349
633 nm. For high-magnification images, the defocus was $-8\ \mu\text{m}$. Cell width and
634 peptidoglycan width were measured using Fiji ⁷⁰. Measurement of cell width was
635 straightforward. For PG width, small sections (about 50 nm) of cell envelope images
636 were excised, rotated so that envelope layers were vertical, and the Plot Profile tool
637 was used to measure the width of the base of the peak corresponding to the PG layer.
638 Dose-symmetric tilt series were collected on a 300kV Titan Krios (Thermo Fisher
639 Scientific) transmission electron microscope equipped with a Quantum LS imaging
640 filter (Gatan, with slit width of 20 eV), single-tilt axis holder and K3 direct electron
641 detector (Gatan). Tilt series with an angular increment of 2° and an angular range of
642 $\pm 60^\circ$ were acquired with the Tomography software (Thermo Fisher Scientific), version
643 5.2.0.5806REL. The total electron dose was 130 electrons per \AA^2 at a pixel size of 8 \AA .
644 Dose symmetric tilt series were saved as separate stacks of frames and subsequently
645 motion-corrected and re-stacked from -60° to $+60^\circ$ using IMOD's function align
646 frames ⁷¹ with the help of a homemade bash script. Three-dimensional reconstructions
647 were calculated in IMOD 4.9.10 by weighted back projection and a gaussian filter was
648 used to enhance contrast and facilitate subsequent segmentation analysis. The 3D

649 segmentation of the tomograms was performed by using the Amira 2020.2 software
650 (Thermo Fisher Scientific).

651 It should be noted that only a subpopulation of the triple mutant could be
652 analyzed due to the frequent rupture of the fragile large vesicles during the blotting
653 step of the sample preparation.

654

655 **DATA AVAILABILITY STATEMENT**

656 The authors declare that all data supporting the findings of this study are available
657 within the paper and its supplementary information files (source data for figures 2, 3a,
658 extended data figures 1, 2a, 3, 5a, 6a and supplementary data for supplementary
659 figures S1a,b and S2a,b) or, otherwise, are available from the corresponding author
660 upon request.

661

662 **ACKNOWLEDGEMENTS**

663 This work was supported by funding from the French National Research Agency
664 (ANR) (Fir-OM ANR-16-CE12-0010), the Institut Pasteur “Programmes Transversaux
665 de Recherche” (PTR 39-16), the French government's Investissement d'Avenir
666 Program, Laboratoire d'Excellence "Integrative Biology of Emerging Infectious
667 Diseases" (grant n°ANR-10-LABX-62-IBEID) and the Fondation pour la Recherche
668 Médicale (grant DEQ20180339185). N.P. is funded by a Pasteur-Roux Postdoctoral
669 Fellowship from the Institut Pasteur. We thank Alicia Jiménez-Fernández for help with
670 *Veillonella* genetics techniques. We gratefully acknowledge the UTechS Photonic
671 BioImaging (Imagopole), C2RT, Institut Pasteur (Paris, France) and the France–
672 BioImaging infrastructure network supported by the French National Research
673 Agency (ANR-10-INSB-04; Investments for the Future), and the Région Ile-de-France
674 (program Domaine d'Intérêt Majeur-Malinf) for the use of the Zeiss LSM 780 Elyra PS1

675 microscope. We thank S. Tachon from the NanoImaging Core facility of the Center for
676 Technological Resources and Research of Institut Pasteur for assistance with the
677 tomography acquisitions at the Titan Krios microscope. We are grateful for equipment
678 support from the French Government Programme Investissements d’Avenir France
679 BioImaging (FBI, N° ANR-10-INSB-04-01). We thank M. Nilges and the Equipex
680 CACSICE (Centre d’analyse de systèmes complexes dans les environnements
681 complexes) for providing the Falcon II direct detector. The authors acknowledge the
682 IT department at Institut Pasteur, Paris, for providing computational and storage
683 services (TARS cluster).

684

685

686 **AUTHORS CONTRIBUTIONS STATEMENT**

687 JW performed all molecular biology and microbiology experiments with the assistance
688 of TNT. ASR and JW performed the electron microscopy data acquisition,
689 reconstructions and visualizations. NP performed the 3D-SIM data acquisition and
690 treatment and drew the schematic representations (Figures 1 and 6). NT and JW
691 performed the bioinformatic and evolutionary analysis. DP performed preliminary
692 bioinformatic analyses in an early version of the manuscript. JMG provided lab
693 facilities. CB and SG supervised the study. JW, CB and SG wrote the paper with
694 contributions from ASR, NT, NP, and JMG. All authors contributed to the final version
695 of the manuscript.

696

697 **COMPETING INTEREST STATEMENT**

698 All the authors declare that they have no competing interests

699

700 **FIGURE LEGENDS**

701

702 **Figure 1. Schematic representation of the four major mechanisms for OM**
703 **attachment to the cell wall: (a)** Lpp, Pal and OmpA as the canonical *E. coli* systems,
704 and OmpM as an alternative system reported from some Terrabacteria; **(b)** domain
705 organization of the corresponding proteins. LPS means lipopolysaccharide, OM –
706 outer membrane, PG – peptidoglycan, SS – signal sequence.

707

708 **Figure 2. Distribution of major known OM attachment systems mapped on a**
709 **reference phylogeny of Bacteria (a) and on a schematic tree of the Firmicutes (b).** The
710 phylogeny is based on the concatenation of RNA polymerase subunits β , β' and
711 elongation factor IF-2 (2,206 amino-acid positions and 377 taxa) and is rooted in
712 between the two large clades of the Terrabacteria and Gracilicutes, according to
713 ^{4,72}. The tree was calculated using IQ-TREE version 1.6.3 with the model LG+C60+F+G
714 and black dots indicate bootstrap values >90%. The presence of each of the four main
715 attachment systems, of the Lol system, and of CsaB/SLH is marked with a colored dot.
716 Arrows indicate the possible origin of each system. Red cross indicates the OM loss.
717 The question mark in the LBCA indicates uncertainty on the presence of OmpM or
718 OmpA (or yet another mechanism) (see Figure 6). Note that D indicates the presence
719 of a classical OM (with or without LPS) as inferred either by experimental data or by
720 the presence of Bam and other known OM systems. For this reason, Actinobacteria are
721 marked as monoderms (M) even if some members have an OM made of mycolic acids,
722 which is of more recent origin. In parentheses are indicated the number of genomes
723 analyzed. All accession numbers are given in Supplementary Data Sheet 1A and 1B.
724 The phylogenetic tree is available as a Newick file (Source Data for Figure 2.newick).

725

726 **Figure 3. Phenotype of different *V. parvula* mutants generated in this study as**
727 **compared to the WT. (a)** – Growth curves. All data points represent the mean of a
728 pentaplicate, error bars were omitted for sake of visibility. Cultures were made in
729 BHILC medium in 96-well plates at 37°C under anaerobic conditions. **(b)** –
730 Epifluorescence observation of cells labelled with the biological membrane staining
731 dye FM 4-64 (Thermo Fisher Scientific). All scale bars represent 5 μm . The samples
732 shown are representative of multiple (n>10) experiments.

733

734 **Figure 4. Membrane and DNA staining of representative *V. parvula* WT and**
735 **$\Delta\text{ompM1-3}$ mutant cells imaged by 3D SIM.** Cell membranes were stained with by
736 FM4-64 (red) and the DNA by DAPI (blue). **(a)** *V. parvula* WT. **(b and c)** $\Delta\text{ompM1-3}$
737 mutant of *V. parvula*; the panel **(b)** presents a large field of view where arrows indicate
738 vesicles of different sizes devoid of any DNA signal. **(d)** $\Delta\text{ompM1-3}$ mutant of *V.*
739 *parvula* complemented with pJW35 vector expressing OmpM1-HA under control of a
740 *tet* promoter, induced overnight with 250 $\mu\text{g}/\text{l}$ of anhydrotetracycline (+ATC). **(e)**
741 $\Delta\text{ompM1-3}$ mutant of *V. parvula* complemented with an uninduced pJW35 vector (-
742 ATC). Inlet shows membrane vesicles without DNA content. Scale bar in all images is
743 1 μm . The 3D-SIM acquisition was performed once, but the phenotype of the shown
744 samples, as assessed by conventional fluorescence microscopy, is representative of
745 multiple (n>20) experiments.

746

747 **Figure 5. Cryo-electron tomography of *V. parvula* WT and mutant cells. (a)** – WT, **(b-**
748 **c)** – $\Delta\text{ompM1-3}$ mutant; detached outer membrane forming blebs and vesicles is well
749 visible, **(d)** - $\Delta\text{ompM1-3}$ mutant of *V. parvula* complemented with pJW35 vector
750 (expressing OmpM1-HA under control of *tet* promoter) induced overnight with 250

751 $\mu\text{g}/\text{l}$ of anhydrotetracycline. Left panels represent a sum of 10 tomogram slices (16
752 nm), right panels a 3D rendering of the cell envelope structure based on manual
753 segmentation of tomogram slices, middle panels are the superposition of a tomogram
754 slice and the 3D rendering. OM / blue marking – outer membrane, PG / red marking
755 – peptidoglycan, IM / green marking – inner membrane. White arrows show OM
756 tubules. Pink arrows show a bundle of fimbriae-like structures connecting two OM.
757 Yellow asterisk shows a degraded cell. Cyan arrows show bacteriophages (see
758 Supplementary Results and Discussion 4). All scale bars represent $0.5 \mu\text{m}$. Videos
759 corresponding to panels a to d, containing all slices of the 3D tomogram reconstruction
760 are available as Supplementary Movies S1 to S4. The CryoEM acquisition was
761 performed twice, but the phenotype of the presented samples, as assessed by
762 conventional fluorescence microscopy, is representative of multiple ($n>20$)
763 experiments. The presence of phages, as visible in some Cryo-ET images, is not
764 responsible for the observed phenotypes (see Supplementary Discussion).

765

766 **Figure 6. Two scenarios of evolution of OM tethering in Bacteria.** Acquisitions are
767 marked with full line arrows, and losses with dotted line arrows. In scenario 1, the
768 LBCA tethered its OM via OmpM, and through interaction of the SLH domain with
769 secondary cell wall polymers (SCWP) pyruvylated by the CsaB enzyme; this cell
770 envelope configuration was inherited in diderm Terrabacteria, whereas in Gracilicutes
771 the SLH domain was replaced by an OmpA domain leading to the OmpA tethering
772 system, and the pyruvylated secondary cell wall polymers were lost along with CsaB.
773 In scenario 2, the LBCA tethered its OM via OmpA; in Terrabacteria, the OmpA
774 domain was replaced by the SLH domain upon appearance of the CsaB enzyme
775 pyruvylating the SCWP, leading to the OmpM tethering system, whereas OmpA was

776 conserved in Gracilicutes. In both scenarios, Pal arose from OmpA by replacement of
777 the porin domain with a lipid tail upon appearance of the Lol system to address
778 lipoproteins to the OM. Finally, Lpp appeared *de novo* within *Gammaproteobacteria*.

779

780 References

781

- 782 1. Megrian, D., Taib, N., Witwinowski, J., Beloin, C. & Gribaldo, S. One or two
783 membranes? Diderm Firmicutes challenge the Gram-positive/Gram-negative divide. *Mol.*
784 *Microbiol.* **113**, 659–671 (2020).
- 785 2. Tocheva, E. I., Ortega, D. R. & Jensen, G. J. Sporulation, bacterial cell envelopes and
786 the origin of life. *Nat. Rev. Microbiol.* **14**, 535–542 (2016).
- 787 3. Taib, N. *et al.* Genome-wide analysis of the Firmicutes illuminates the
788 diderm/monoderm transition. *Nat. Ecol. Evol.* **4**, 1661–1672 (2020).
- 789 4. Coleman, G. A. *et al.* A rooted phylogeny resolves early bacterial evolution. *Science*
790 **372**, (2021).
- 791 5. Cavalier-Smith, T. The neomuran origin of archaeobacteria, the negibacterial root of the
792 universal tree and bacterial megaclassification. *Int. J. Syst. Evol. Microbiol.* **52**, 7–76 (2002).
- 793 6. Braun, V. & Rehn, K. Chemical characterization, spatial distribution and function of a
794 lipoprotein (murein-lipoprotein) of the *E. coli* cell wall. The specific effect of trypsin on the
795 membrane structure. *Eur. J. Biochem.* **10**, 426–438 (1969).
- 796 7. Braun, V. Covalent lipoprotein from the outer membrane of *Escherichia coli*. *Biochim.*
797 *Biophys. Acta* **415**, 335–377 (1975).
- 798 8. Suzuki, H. *et al.* Murein-lipoprotein of *Escherichia coli*: a protein involved in the
799 stabilization of bacterial cell envelope. *Mol. Gen. Genet. MGG* **167**, 1–9 (1978).
- 800 9. Yem, D. W. & Wu, H. C. Physiological characterization of an *Escherichia coli* mutant
801 altered in the structure of murein lipoprotein. *J. Bacteriol.* **133**, 1419–1426 (1978).
- 802 10. Cascales, E., Bernadac, A., Gavioli, M., Lazzaroni, J.-C. & Lloubes, R. Pal lipoprotein
803 of *Escherichia coli* plays a major role in outer membrane integrity. *J. Bacteriol.* **184**, 754–759
804 (2002).
- 805 11. Cohen, E. J., Ferreira, J. L., Ladinsky, M. S., Beeby, M. & Hughes, K. T. Nanoscale-
806 length control of the flagellar driveshaft requires hitting the tethered outer membrane. *Science*
807 **356**, 197–200 (2017).
- 808 12. Bouveret, E., Bénédicti, H., Rigal, A., Loret, E. & Lazdunski, C. In vitro
809 characterization of peptidoglycan-associated lipoprotein (PAL)-peptidoglycan and PAL-TolB
810 interactions. *J. Bacteriol.* **181**, 6306–6311 (1999).
- 811 13. Parsons, L. M., Lin, F. & Orban, J. Peptidoglycan recognition by Pal, an outer
812 membrane lipoprotein. *Biochemistry* **45**, 2122–2128 (2006).
- 813 14. Bernadac, A., Gavioli, M., Lazzaroni, J. C., Raina, S. & Lloubès, R. *Escherichia coli*
814 tol-pal mutants form outer membrane vesicles. *J. Bacteriol.* **180**, 4872–4878 (1998).
- 815 15. Gerding, M. A., Ogata, Y., Pecora, N. D., Niki, H. & de Boer, P. A. J. The trans-
816 envelope Tol-Pal complex is part of the cell division machinery and required for proper outer-
817 membrane invagination during cell constriction in *E. coli*. *Mol. Microbiol.* **63**, 1008–1025
818 (2007).
- 819 16. Szczepaniak, J., Press, C. & Kleanthous, C. The multifarious roles of Tol-Pal in Gram-

820 negative bacteria. *FEMS Microbiol. Rev.* **44**, 490–506 (2020).

821 17. Park, J. S. *et al.* Mechanism of anchoring of OmpA protein to the cell wall
822 peptidoglycan of the gram-negative bacterial outer membrane. *FASEB J. Off. Publ. Fed. Am.*
823 *Soc. Exp. Biol.* **26**, 219–228 (2012).

824 18. Samsudin, F., Boags, A., Piggot, T. J. & Khalid, S. Braun's Lipoprotein Facilitates
825 OmpA Interaction with the Escherichia coli Cell Wall. *Biophys. J.* **113**, 1496–1504 (2017).

826 19. Tocheva, E. I. *et al.* Peptidoglycan remodeling and conversion of an inner membrane
827 into an outer membrane during sporulation. *Cell* **146**, 799–812 (2011).

828 20. Antunes, L. C. *et al.* Phylogenomic analysis supports the ancestral presence of LPS-
829 outer membranes in the Firmicutes. *eLife* **5**, (2016).

830 21. Kamio, Y. & Takahashi, H. Outer membrane proteins and cell surface structure of
831 *Selenomonas ruminantium*. *J. Bacteriol.* **141**, 899–907 (1980).

832 22. Kalmokoff, M. L. *et al.* Physical and genetic characterization of an outer-membrane
833 protein (OmpM1) containing an N-terminal S-layer-like homology domain from the
834 phylogenetically Gram-positive gut anaerobe *Mitsuokella multacida*. *Anaerobe* **15**, 74–81
835 (2009).

836 23. Kojima, S. *et al.* Cadaverine covalently linked to peptidoglycan is required for
837 interaction between the peptidoglycan and the periplasm-exposed S-layer-homologous
838 domain of major outer membrane protein Mep45 in *Selenomonas ruminantium*. *J. Bacteriol.*
839 **192**, 5953–5961 (2010).

840 24. Kojima, S. & Kamio, Y. Molecular basis for the maintenance of envelope integrity in
841 *Selenomonas ruminantium*: cadaverine biosynthesis and covalent modification into the
842 peptidoglycan play a major role. *J. Nutr. Sci. Vitaminol. (Tokyo)* **58**, 153–160 (2012).

843 25. Kamio, Y., Itoh, Y. & Terawaki, Y. Chemical structure of peptidoglycan in
844 *Selenomonas ruminantium*: cadaverine links covalently to the D-glutamic acid residue of
845 peptidoglycan. *J. Bacteriol.* **146**, 49–53 (1981).

846 26. Kamio, Y. & Nakamura, K. Putrescine and cadaverine are constituents of
847 peptidoglycan in *Veillonella alcalescens* and *Veillonella parvula*. *J. Bacteriol.* **169**, 2881–
848 2884 (1987).

849 27. Poppleton, D. I. *et al.* Outer Membrane Proteome of *Veillonella parvula*: A Diderm
850 Firmicute of the Human Microbiome. *Front. Microbiol.* **8**, 1215 (2017).

851 28. Hansel, A. & Tadros, M. H. Characterization of two pore-forming proteins isolated
852 from the outer membrane of *Synechococcus* PCC 6301. *Curr. Microbiol.* **36**, 321–326 (1998).

853 29. Kojima, S. & Okumura, Y. Outer membrane-deprived cyanobacteria liberate
854 periplasmic and thylakoid luminal components that support the growth of heterotrophs.
855 *bioRxiv* 2020.03.24.006684 (2020) doi:10.1101/2020.03.24.006684.

856 30. Fernández-Herrero, L. A., Olabarria, G., Castón, J. R., Lasa, I. & Berenguer, J.
857 Horizontal transference of S-layer genes within *Thermus thermophilus*. *J. Bacteriol.* **177**,
858 5460–5466 (1995).

859 31. Olabarria, G., Carrascosa, J. L., de Pedro, M. A. & Berenguer, J. A conserved motif in
860 S-layer proteins is involved in peptidoglycan binding in *Thermus thermophilus*. *J. Bacteriol.*
861 **178**, 4765–4772 (1996).

862 32. Cava, F., de Pedro, M. A., Schwarz, H., Henne, A. & Berenguer, J. Binding to
863 pyruvylated compounds as an ancestral mechanism to anchor the outer envelope in primitive
864 bacteria. *Mol. Microbiol.* **52**, 677–690 (2004).

865 33. Engel, A. M., Cejka, Z., Lupas, A., Lottspeich, F. & Baumeister, W. Isolation and
866 cloning of Omp alpha, a coiled-coil protein spanning the periplasmic space of the ancestral
867 eubacterium *Thermotoga maritima*. *EMBO J.* **11**, 4369–4378 (1992).

- 868 34. Egan, A. J. F. Bacterial outer membrane constriction. *Mol. Microbiol.* **107**, 676–687
869 (2018).
- 870 35. Asmar, A. T. & Collet, J.-F. Lpp, the Braun lipoprotein, turns 50—major
871 achievements and remaining issues. *FEMS Microbiol. Lett.* **365**, (2018).
- 872 36. Braun, V. & Hantke, K. Lipoproteins: Structure, Function, Biosynthesis. *Subcell.*
873 *Biochem.* **92**, 39–77 (2019).
- 874 37. Mesnage, S. *et al.* Bacterial SLH domain proteins are non-covalently anchored to the
875 cell surface via a conserved mechanism involving wall polysaccharide pyruvylation. *EMBO J.*
876 **19**, 4473–4484 (2000).
- 877 38. Kojima, S. *et al.* Peptidoglycan-associated outer membrane protein Mep45 of rumen
878 anaerobe *Selenomonas ruminantium* forms a non-specific diffusion pore via its C-terminal
879 transmembrane domain. *Biosci. Biotechnol. Biochem.* **80**, 1954–1959 (2016).
- 880 39. Farci, D. *et al.* Structural insights into the main S-layer unit of *Deinococcus*
881 *radiodurans* reveal a massive protein complex with porin-like features. *J. Biol. Chem.* **295**,
882 4224–4236 (2020).
- 883 40. Pisareva, T. *et al.* Model for Membrane Organization and Protein Sorting in the
884 Cyanobacterium *Synechocystis* sp. PCC 6803 Inferred from Proteomics and Multivariate
885 Sequence Analyses. *J. Proteome Res.* **10**, 3617–3631 (2011).
- 886 41. Heinz, E., Selkig, J., Belousoff, M. J. & Lithgow, T. Evolution of the Translocation
887 and Assembly Module (TAM). *Genome Biol. Evol.* **7**, 1628–1643 (2015).
- 888 42. Webb, C. T., Heinz, E. & Lithgow, T. Evolution of the β -barrel assembly machinery.
889 *Trends Microbiol.* **20**, 612–620 (2012).
- 890 43. Anwari, K. *et al.* The evolution of new lipoprotein subunits of the bacterial outer
891 membrane BAM complex. *Mol. Microbiol.* **84**, 832–844 (2012).
- 892 44. Godessart, P. *et al.* β -Barrels covalently link peptidoglycan and the outer membrane in
893 the α -proteobacterium *Brucella abortus*. *Nat. Microbiol.* **6**, 27–33 (2021).
- 894 45. Sandoz, K. M. *et al.* β -Barrel proteins tether the outer membrane in many Gram-
895 negative bacteria. *Nat. Microbiol.* **6**, 19–26 (2021).
- 896 46. Wang, Y.-H. *et al.* PapA, a peptidoglycan-associated protein, interacts with OmpC and
897 maintains cell envelope integrity. *Environ. Microbiol.* **23**, 600–612 (2021).
- 898 47. Hoppert, M. *et al.* Structure–functional analysis of the *Dictyoglomus* cell envelope.
899 *Syst. Appl. Microbiol.* **35**, 279–290 (2012).
- 900 48. Brock, T. D. & Edwards, M. R. Fine structure of *Thermus aquaticus*, an extreme
901 thermophile. *J. Bacteriol.* **104**, 509–517 (1970).
- 902 49. Gaisin, V. A., Kooger, R., Grouzdev, D. S., Gorlenko, V. M. & Pilhofer, M. Cryo-
903 Electron Tomography Reveals the Complex Ultrastructural Organization of Multicellular
904 Filamentous Chloroflexota (Chloroflexi) Bacteria. *Front. Microbiol.* **11**, 1373 (2020).
- 905 50. van Teeseling, M. C. F. *et al.* Anammox Planctomycetes have a peptidoglycan cell
906 wall. *Nat. Commun.* **6**, 6878 (2015).
- 907 51. Boedeker, C. *et al.* Determining the bacterial cell biology of Planctomycetes. *Nat.*
908 *Commun.* **8**, 14853 (2017).
- 909 52. Johnson, L. S., Eddy, S. R. & Portugaly, E. Hidden Markov model speed heuristic and
910 iterative HMM search procedure. *BMC Bioinformatics* **11**, 431 (2010).
- 911 53. Tsirigos, K. D., Elofsson, A. & Bagos, P. G. PRED-TMBB2: improved topology
912 prediction and detection of beta-barrel outer membrane proteins. *Bioinforma. Oxf. Engl.* **32**,
913 i665–i671 (2016).
- 914 54. Hayat, S., Peters, C., Shu, N., Tsirigos, K. D. & Elofsson, A. Inclusion of dyad-repeat
915 pattern improves topology prediction of transmembrane β -barrel proteins. *Bioinforma. Oxf.*

916 *Engl.* **32**, 1571–1573 (2016).

917 55. Abby, S. S., Néron, B., Ménager, H., Touchon, M. & Rocha, E. P. C. MacSyFinder: A
918 Program to Mine Genomes for Molecular Systems with an Application to CRISPR-Cas
919 Systems. *PLOS ONE* **9**, e110726 (2014).

920 56. Letunic, I. & Bork, P. Interactive Tree Of Life (iTOL) v4: recent updates and new
921 developments. *Nucleic Acids Res.* **47**, W256–W259 (2019).

922 57. Criscuolo, A. & Gribaldo, S. BMGE (Block Mapping and Gathering with Entropy): a
923 new software for selection of phylogenetic informative regions from multiple sequence
924 alignments. *BMC Evol. Biol.* **10**, 210 (2010).

925 58. Katoh, K. & Standley, D. M. MAFFT multiple sequence alignment software version 7:
926 improvements in performance and usability. *Mol. Biol. Evol.* **30**, 772–780 (2013).

927 59. Capella-Gutiérrez, S., Silla-Martínez, J. M. & Gabaldón, T. trimAl: a tool for
928 automated alignment trimming in large-scale phylogenetic analyses. *Bioinforma. Oxf. Engl.*
929 **25**, 1972–1973 (2009).

930 60. Nguyen, L.-T., Schmidt, H. A., von Haeseler, A. & Minh, B. Q. IQ-TREE: a fast and
931 effective stochastic algorithm for estimating maximum-likelihood phylogenies. *Mol. Biol.*
932 *Evol.* **32**, 268–274 (2015).

933 61. Kalyaanamoorthy, S., Minh, B. Q., Wong, T. K. F., von Haeseler, A. & Jermini, L. S.
934 ModelFinder: fast model selection for accurate phylogenetic estimates. *Nat. Methods* **14**, 587–
935 589 (2017).

936 62. Hoang, D. T., Chernomor, O., von Haeseler, A., Minh, B. Q. & Vinh, L. S. UFBoot2:
937 Improving the Ultrafast Bootstrap Approximation. *Mol. Biol. Evol.* **35**, 518–522 (2018).

938 63. Green, M. R. & Sambrook, J. *Molecular Cloning: A Laboratory Manual*. (Cold Spring
939 Harbor Laboratory Press., 2012).

940 64. Knapp, S. *et al.* Natural Competence Is Common among Clinical Isolates of
941 *Veillonella parvula* and Is Useful for Genetic Manipulation of This Key Member of the Oral
942 Microbiome. *Front. Cell. Infect. Microbiol.* **7**, 139 (2017).

943 65. Béchon, N. *et al.* Autotransporters Drive Biofilm Formation and Autoaggregation in
944 the Diderm Firmicute *Veillonella parvula*. *J. Bacteriol.* **202**, (2020).

945 66. Inoue, H., Nojima, H. & Okayama, H. High efficiency transformation of *Escherichia*
946 *coli* with plasmids. *Gene* **96**, 23–28 (1990).

947 67. Jacques, I. B. *et al.* Analysis of 51 cyclodipeptide synthases reveals the basis for
948 substrate specificity. *Nat. Chem. Biol.* **11**, 721–727 (2015).

949 68. Robey, R. B., Sharma, R. C. & Schimke, R. T. Preparation of electrocompetent *E. coli*
950 using salt-free growth medium. *BioTechniques* **20**, 42–44 (1996).

951 69. Fagan, R. P. & Fairweather, N. F. *Clostridium difficile* has two parallel and essential
952 Sec secretion systems. *J. Biol. Chem.* **286**, 27483–27493 (2011).

953 70. Schindelin, J. *et al.* Fiji: an open-source platform for biological-image analysis. *Nat.*
954 *Methods* **9**, 676–682 (2012).

955 71. Mastronarde, D. N. & Held, S. R. Automated tilt series alignment and tomographic
956 reconstruction in IMOD. *J. Struct. Biol.* **197**, 102–113 (2017).

957 72. Raymann, K., Brochier-Armanet, C. & Gribaldo, S. The two-domain tree of life is
958 linked to a new root for the Archaea. *Proc. Natl. Acad. Sci. U. S. A.* **112**, 6670–6675 (2015).

959

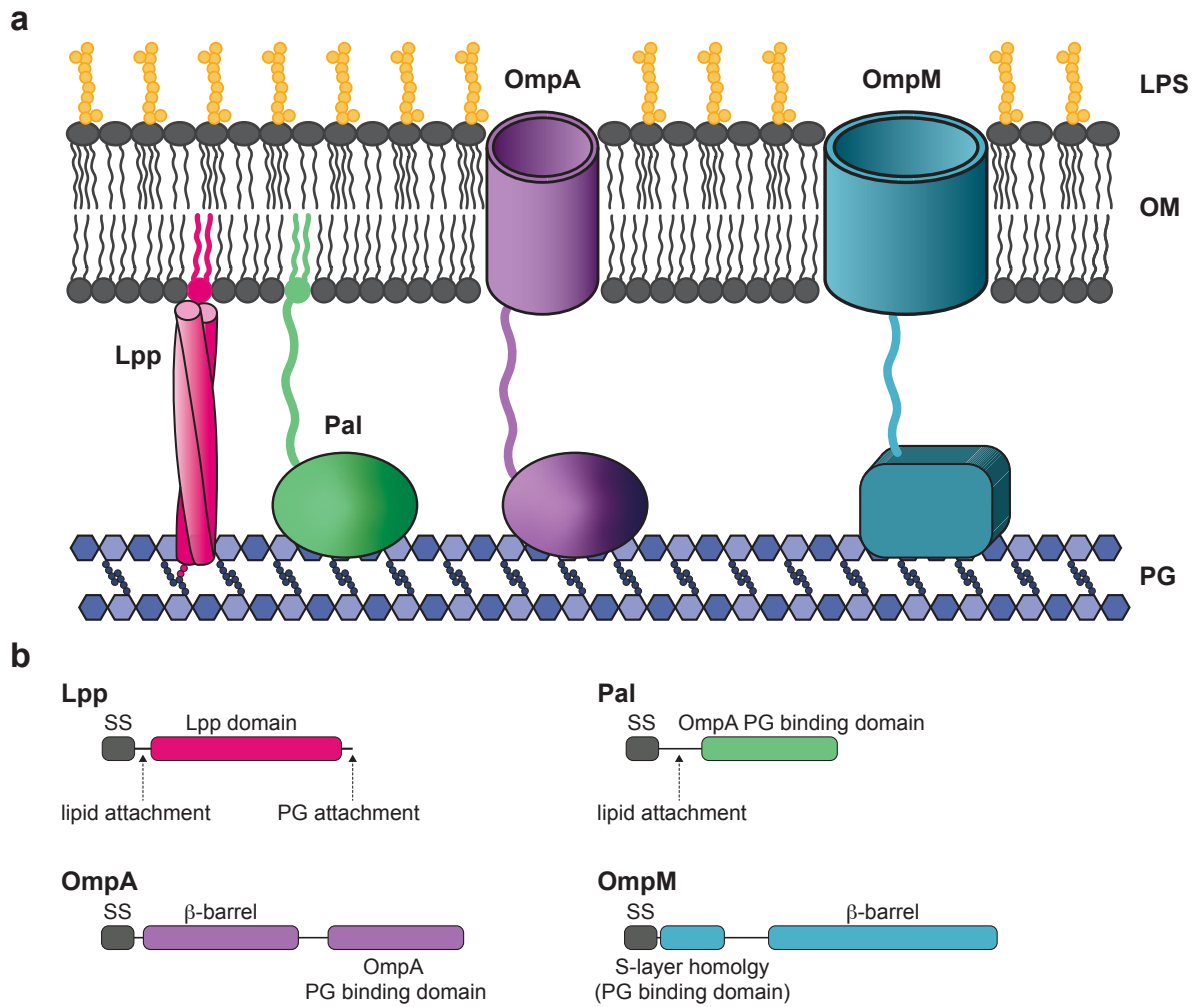


Figure 1. Schematic representation of the four major mechanisms for OM attachment to the cell wall: (a) Lpp, Pal and OmpA as the canonical *E. coli* systems, and OmpM as an alternative system reported from some Terrabacteria; (b) domain organization of the corresponding proteins. LPS means lipopolysaccharide, OM – outer membrane, PG – peptidoglycan, SS – signal sequence.

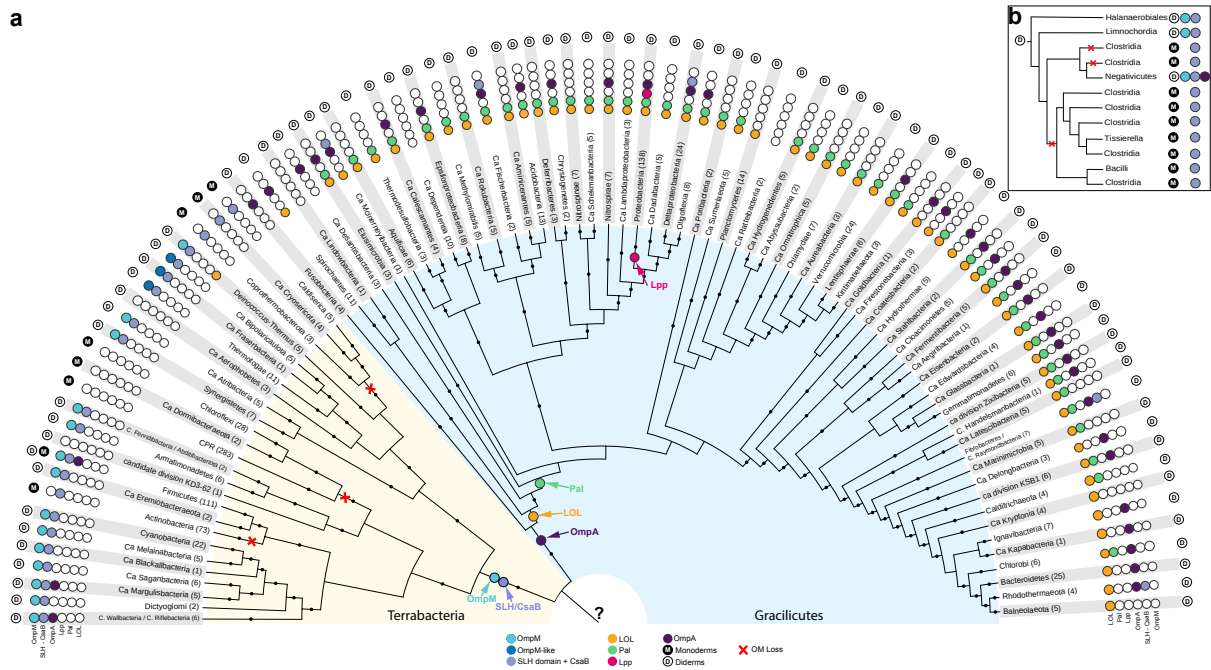


Figure 2. Distribution of major known OM attachment systems mapped on a reference phylogeny of Bacteria (a) and on a schematic tree of the Firmicutes (b). The phylogeny is based on the concatenation of RNA polymerase subunits β , β' and elongation factor IF-2 (2,206 amino-acid positions and 377 taxa) and is rooted in between the two large clades of the Terrabacteria and Gracilicutes, according to 4,72. The tree was calculated using IQ-TREE version 1.6.3 with the model LG+C60+F+G and black dots indicate bootstrap values >90%. The presence of each of the four main attachment systems, of the Lol system, and of CsaB/SLH is marked with a colored dot. Arrows indicate the possible origin of each system. Red cross indicates the OM loss. The question mark in the LBCA indicates uncertainty on the presence of OmpM or OmpA (or yet another mechanism) (see Figure 6). Note that D indicates the presence of a classical OM (with or without LPS) as inferred either by experimental data or by the presence of Bam and other known OM systems. For this reason, Actinobacteria are marked as monoderms (M) even if some members have an OM made of mycolic acids, which is of more recent origin. In parentheses are indicated the number of genomes analyzed. All accession numbers are given in Supplementary Data Sheet 1A and 1B. The phylogenetic tree is available as a Newick file (Source Data for Figure 2.newick).

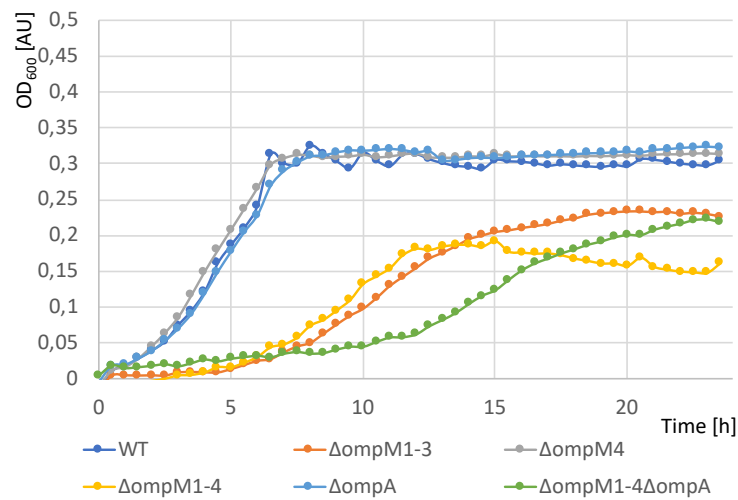
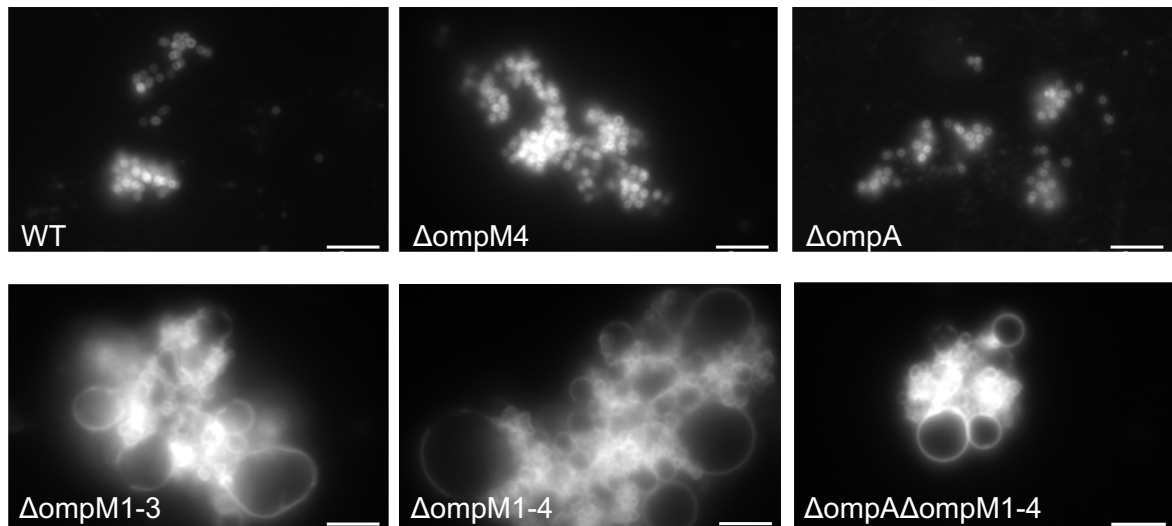
a**b**

Figure 3. Phenotype of different *V. parvula* mutants generated in this study as compared to the WT. (a) – Growth curves. All data points represent the mean of a pentaplicate, error bars were omitted for sake of visibility. Cultures were made in BHILC medium in 96-well plates at 37°C under anaerobic conditions. (b) – Epifluorescence observation of cells labelled with the biological membrane staining dye FM 4-64 (Thermo Fisher Scientific). All scale bars represent 5 μm . The samples shown are representative of multiple (n>10) experiments.

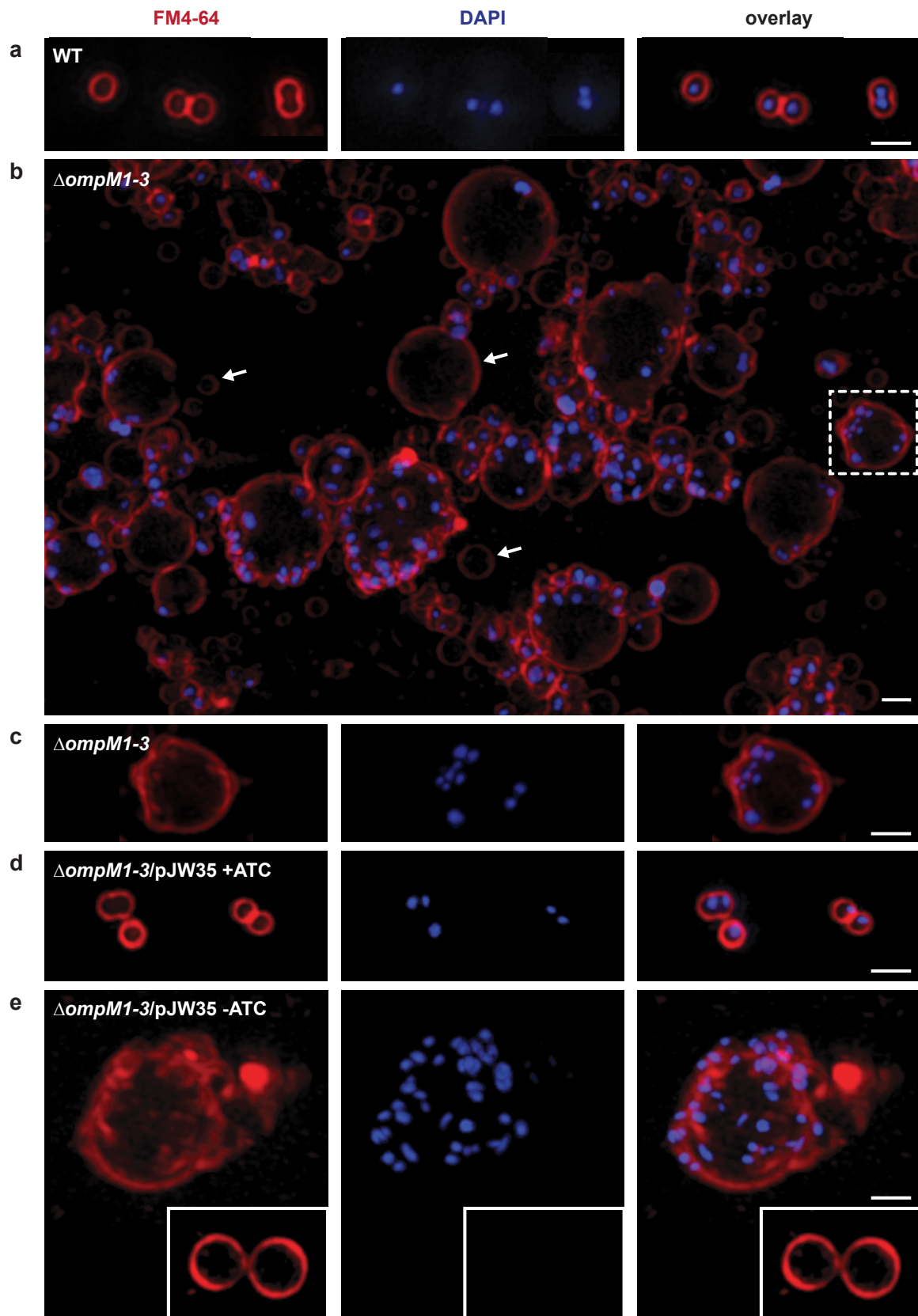


Figure 4. Membrane and DNA staining of representative *V. parvula* WT and $\Delta ompM1-3$ mutant cells imaged by 3D SIM. Cell membranes were stained with by

FM4-64 (red) and the DNA by DAPI (blue). **(a)** *V. parvula* WT. **(b and c)** $\Delta ompM1-3$ mutant of *V. parvula*; the panel **(b)** presents a large field of view where arrows indicate vesicles of different sizes devoid of any DNA signal. **(d)** $\Delta ompM1-3$ mutant of *V. parvula* complemented with pJW35 vector expressing OmpM1-HA under control of a *tet* promoter, induced overnight with 250 $\mu\text{g}/\text{l}$ of anhydrotetracycline (+ATC). **(e)** $\Delta ompM1-3$ mutant of *V. parvula* complemented with an uninduced pJW35 vector (-ATC). Inlet shows membrane vesicles without DNA content. Scale bar in all images is 1 μm . The 3D-SIM acquisition was performed once, but the phenotype of the shown samples, as assessed by conventional fluorescence microscopy, is representative of multiple ($n > 20$) experiments.

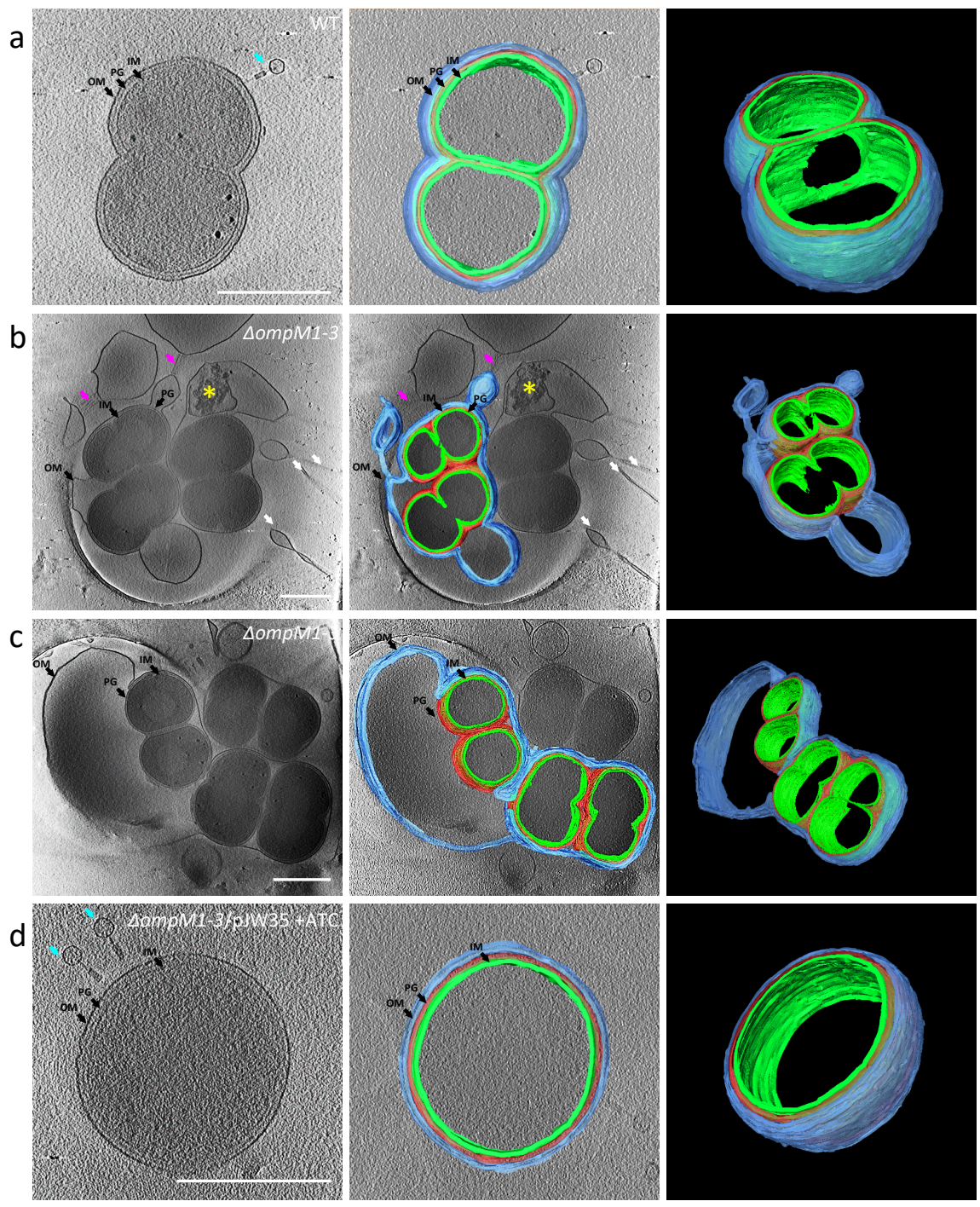


Figure 5. Cryo-electron tomography of *V. parvula* WT and mutant cells. (a) – WT, (b-c) – $\Delta ompM1-3$ mutant; detached outer membrane forming blebs and vesicles is well visible, (d) - $\Delta ompM1-3$ mutant of *V. parvula* complemented with pJW35 vector (expressing OmpM1-HA under control of *tet* promoter) induced overnight with 250 $\mu\text{g}/\text{l}$ of anhydrotetracycline. Left panels represent a sum of 10 tomogram slices (16 nm), right panels a 3D rendering of the cell envelope structure based on manual segmentation of tomogram slices, middle panels are the superposition of a tomogram slice and the 3D rendering. OM / blue marking – outer membrane, PG / red marking – peptidoglycan, IM / green marking – inner membrane. White arrows show OM tubules. Pink arrows show a bundle of fimbriae-like structures connecting two OM. Yellow asterisk shows a degraded cell. Cyan arrows show bacteriophages (see Supplementary Results and Discussion 4). All scale bars represent 0.5 μm . Videos corresponding to panels a to d, containing all slices of the 3D tomogram reconstruction are available as Supplementary Movies S1 to S4. The CryoEM acquisition was performed twice, but the phenotype of the presented samples, as assessed by conventional fluorescence microscopy, is representative of multiple ($n > 20$) experiments. The presence of phages, as visible in some Cryo-ET images, is not responsible for the observed phenotypes (see Supplementary Discussion).

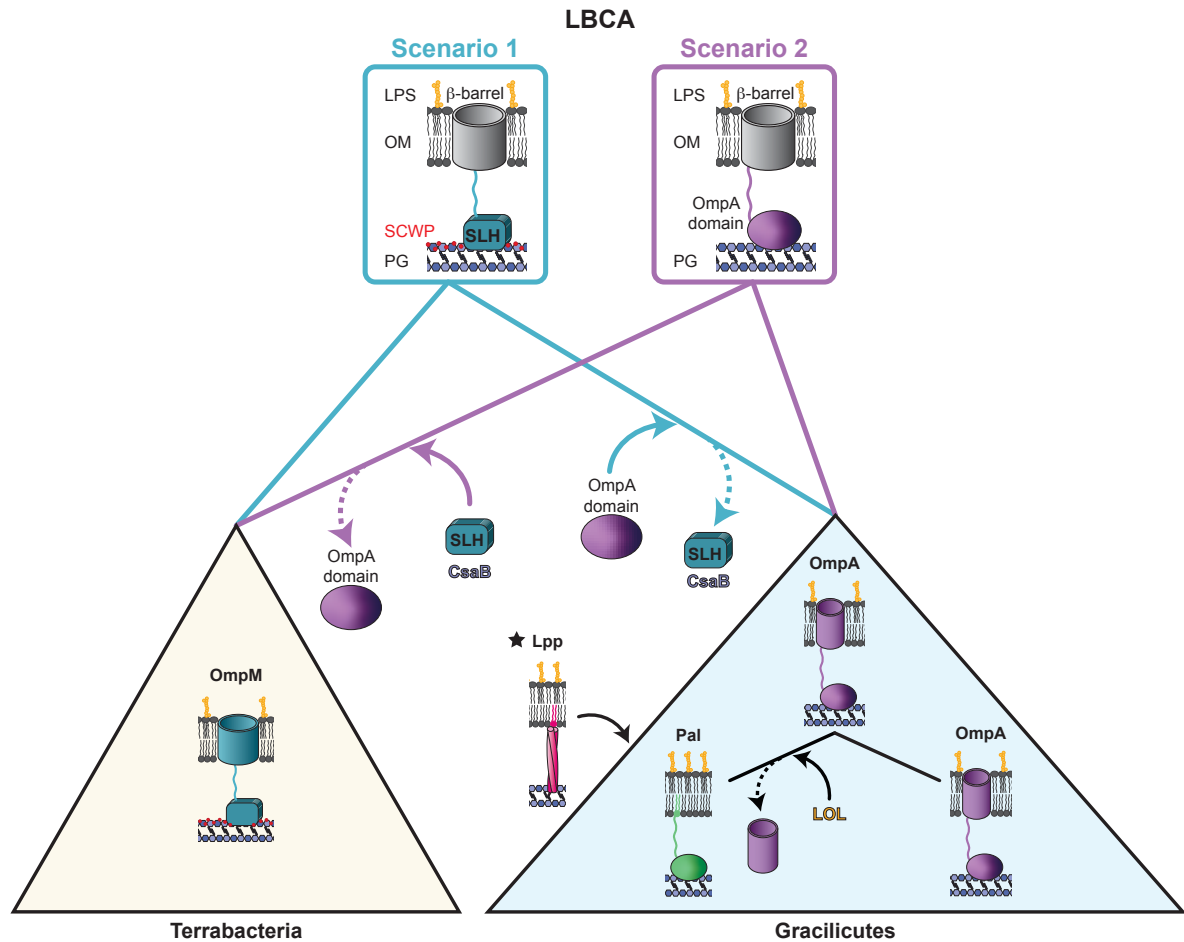
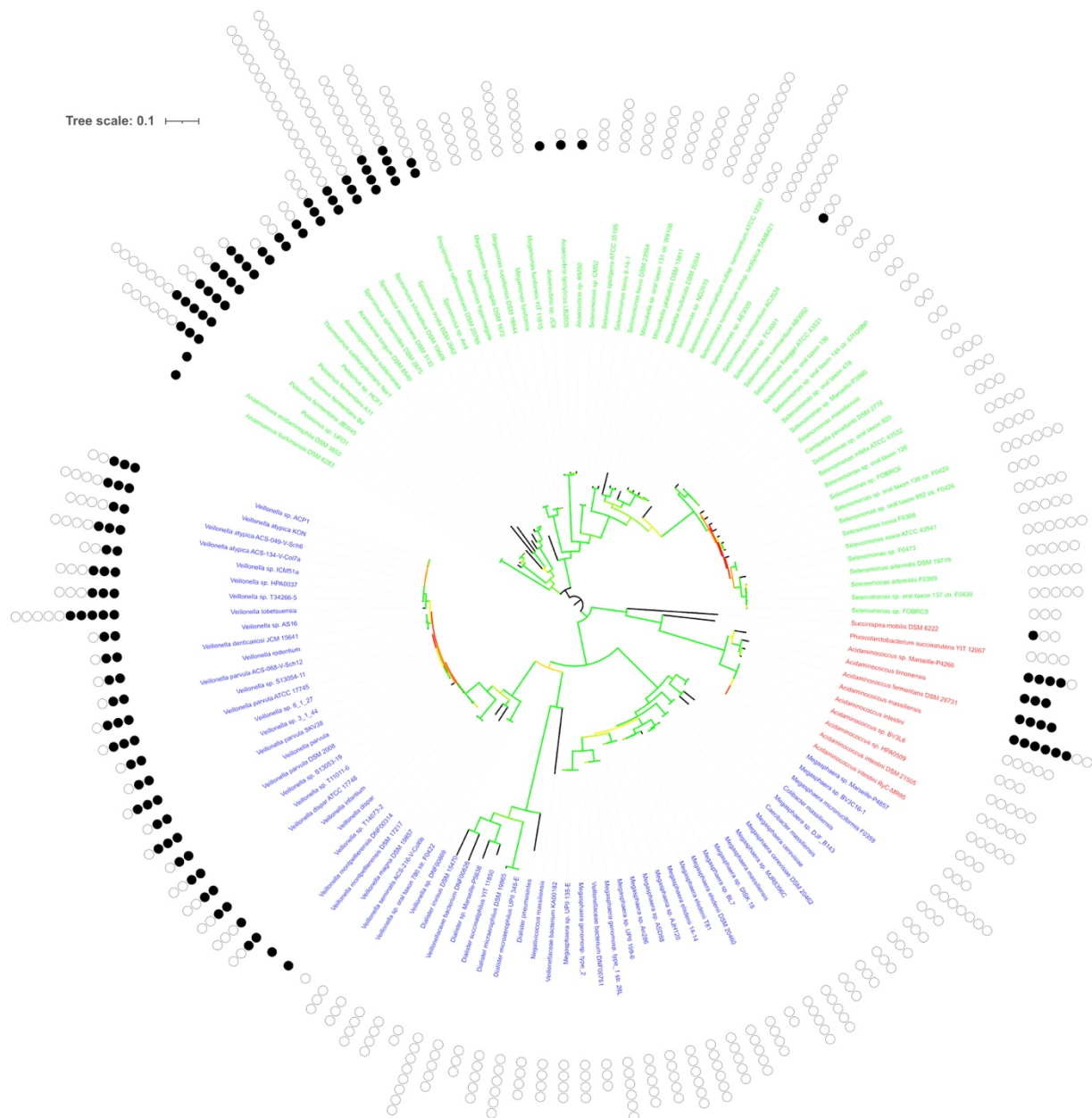


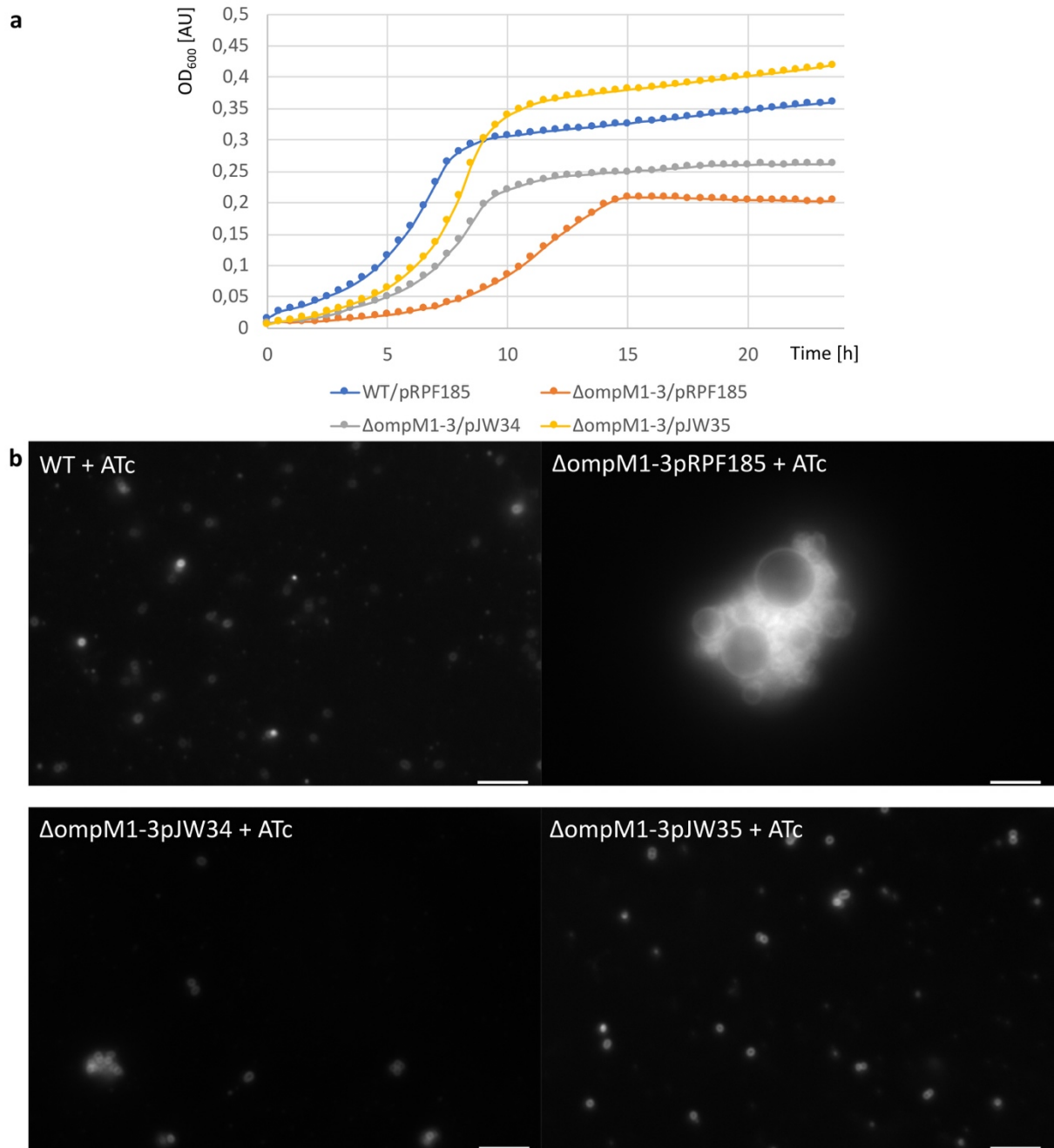
Figure 6. Two scenarios of evolution of OM tethering in Bacteria. Acquisitions are marked with full line arrows, and losses with dotted line arrows. In scenario 1, the LBCA tethered its OM via OmpM, and through interaction of the SLH domain with secondary cell wall polymers (SCWP) pyruvylated by the CsaB enzyme; this cell envelope configuration was inherited in diderm Terrabacteria, whereas in Gracilicutes the SLH domain was replaced by an OmpA domain leading to the OmpA tethering system, and the pyruvylated secondary cell wall polymers were lost along with CsaB. In scenario 2, the LBCA tethered its OM via OmpA; in Terrabacteria, the OmpA domain was replaced by the SLH domain upon appearance of the CsaB enzyme pyruvylating the SCWP, leading to the OmpM tethering system, whereas OmpA was conserved in Gracilicutes. In both scenarios, Pal arose from OmpA by replacement of

the porin domain with a lipid tail upon appearance of the Lol system to address lipoproteins to the OM. Finally, Lpp appeared *de novo* within *Gammaproteobacteria*.



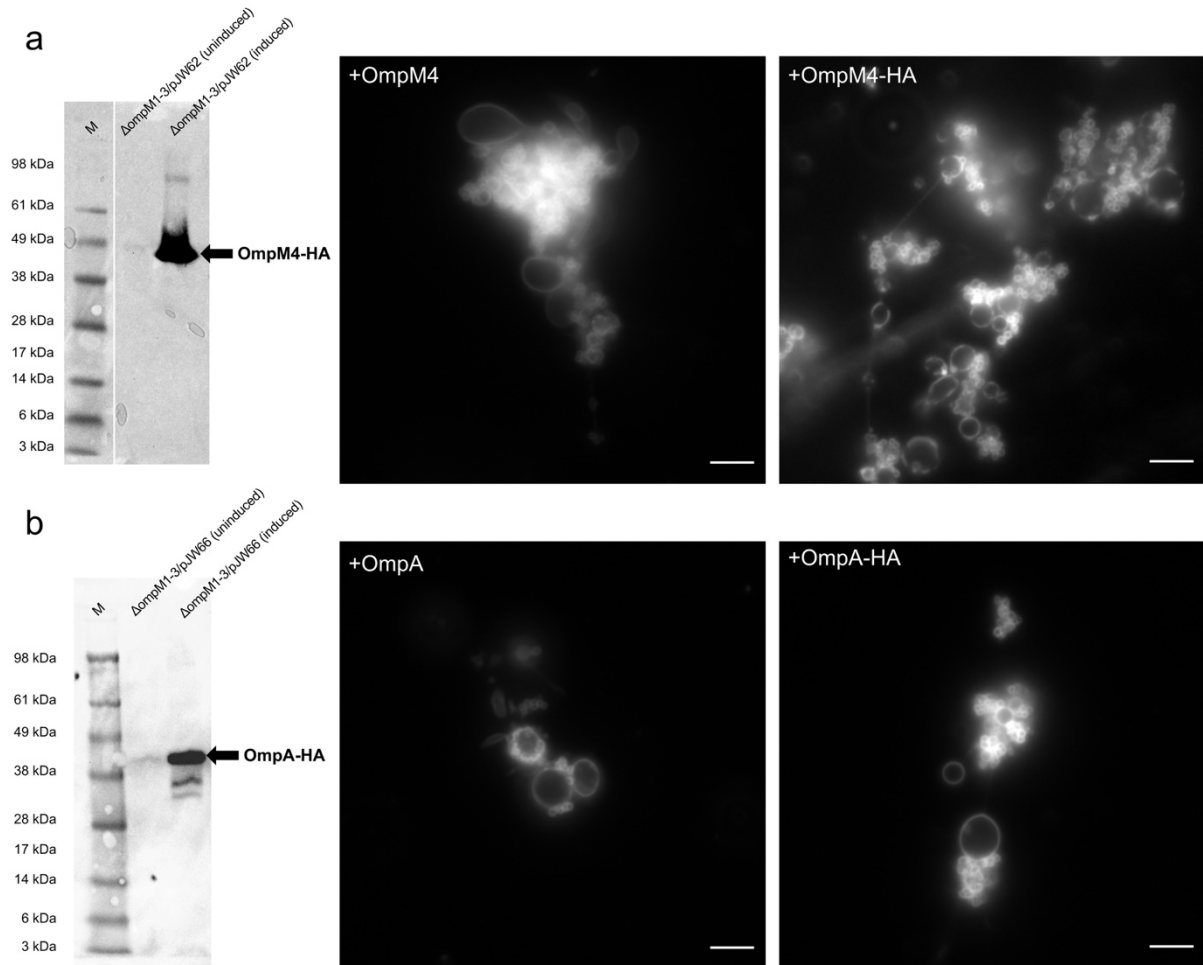
Extended Data Figure 1. Number of *ompM* copies per genome plotted on a reference *Negativicutes* tree containing 135 genomes. Selenomonadales are labelled in green, Acidaminococcales in red and Veillonellales in blue. The phylogeny is based on the concatenation of RNA polymerase subunits β , β' and elongation factor IF-2 (3,027 amino-acid positions) The tree was calculated using IQTREE version 1.6.3 with the model LG+R5. Colours of branches represent bootstrap values from 80 (red) to 100 (green). The *ompM* copies present inside the OM gene cluster are marked by full circles,

those outside the cluster by empty ones. Source data is provided in the file "Source Data for Figure ED1.newick".



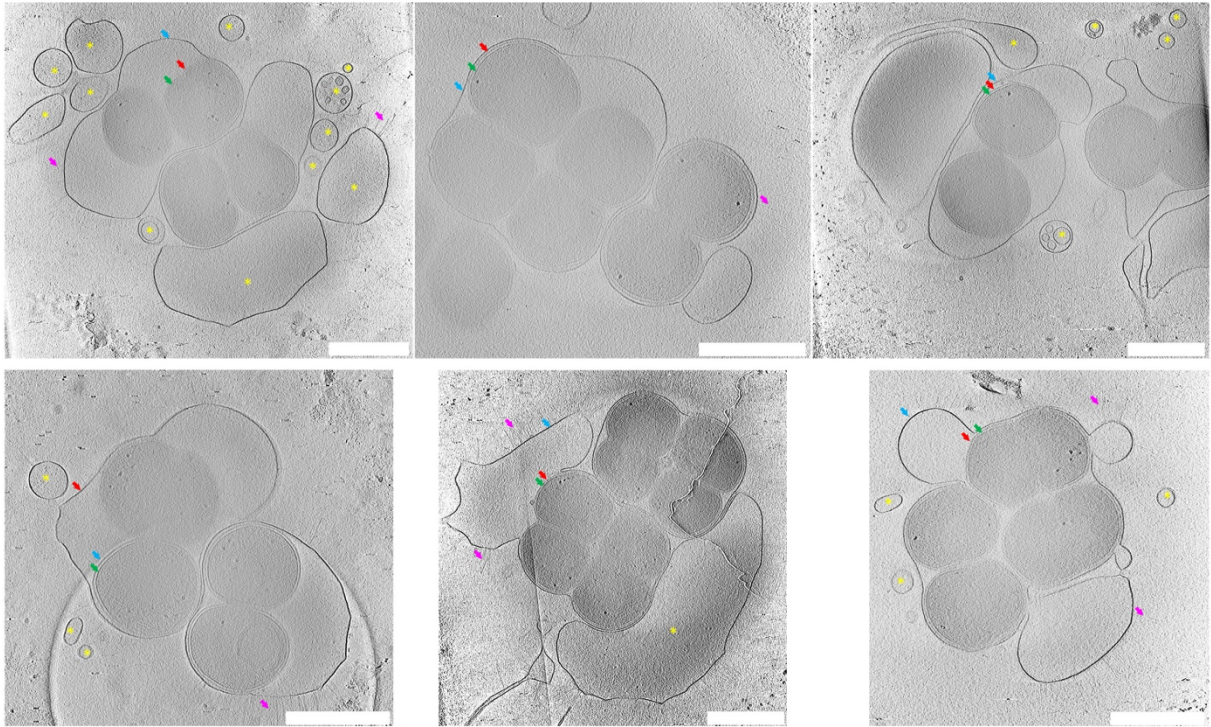
Extended Data Figure 2. Phenotypic complementation of the $\Delta ompM1-3$ mutant by production of native or HA-tagged OmpM1. (a) – Growth curves. All data points represent the mean of a pentaplicate, error bars were omitted for sake of visibility. Cultures were made in BHILC medium in presence of 250 $\mu g/l$ of anhydrotetracycline in 96-well plates at 37°C under anaerobic conditions. pRPF185 – empty vector, pJW34 – a vector expressing native OmpM1 under the control of *tet* promoter, pJW35 – a vector expressing HA-tagged OmpM1 under the control of *tet* promoter. (b) –

Epifluorescence observation of cells labelled with the biological membrane staining dye FM 4-64 (Thermo Fisher Scientific). Overnight cultures were launched at 1/10th dilution of a stationary phase culture in SK medium at 37°C in anaerobic conditions in presence of aTc at 250 µg/l, before being labeled with the biological membrane staining dye FM 4-64 (Thermo Fisher Scientific) and observed by epifluorescence microscopy. Expression of either the native version of OmpM1 or its HA-tagged version led to complementation of the strong phenotype (formation of OM “bubbles” observed in the $\Delta ompM1-3$ mutant). Growth defect of this mutant was also fully or partly complemented by native or HA-tagged OmpM1. All scale bars represent 5 µm. The samples presented are representative of multiple (n>20) experiments.

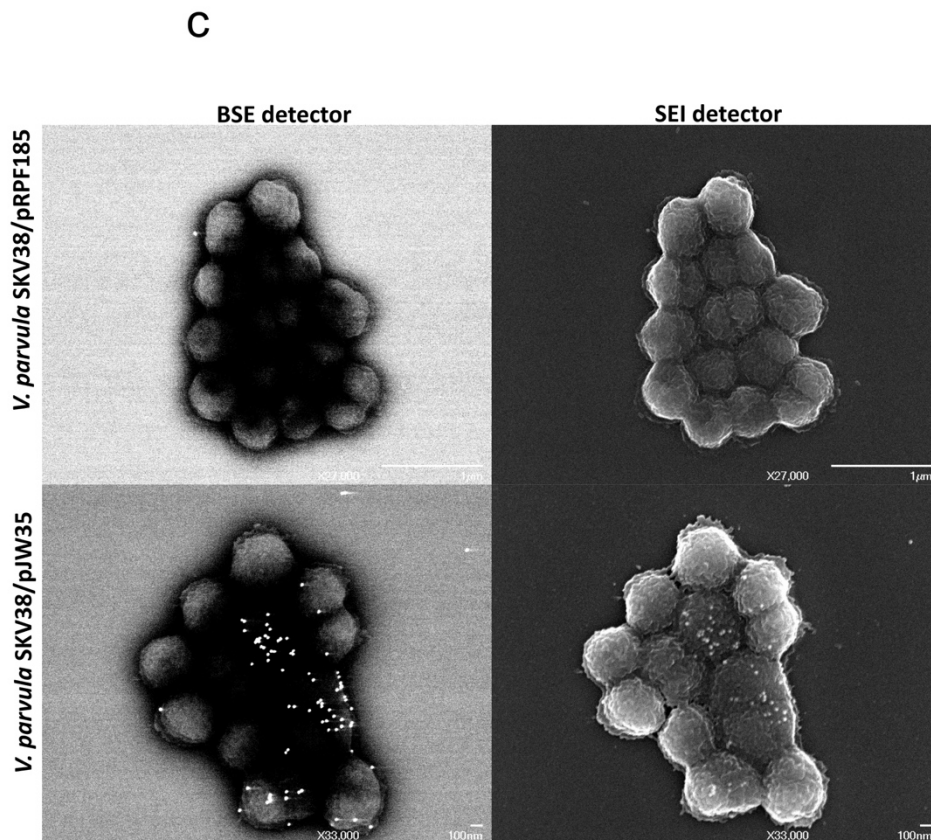
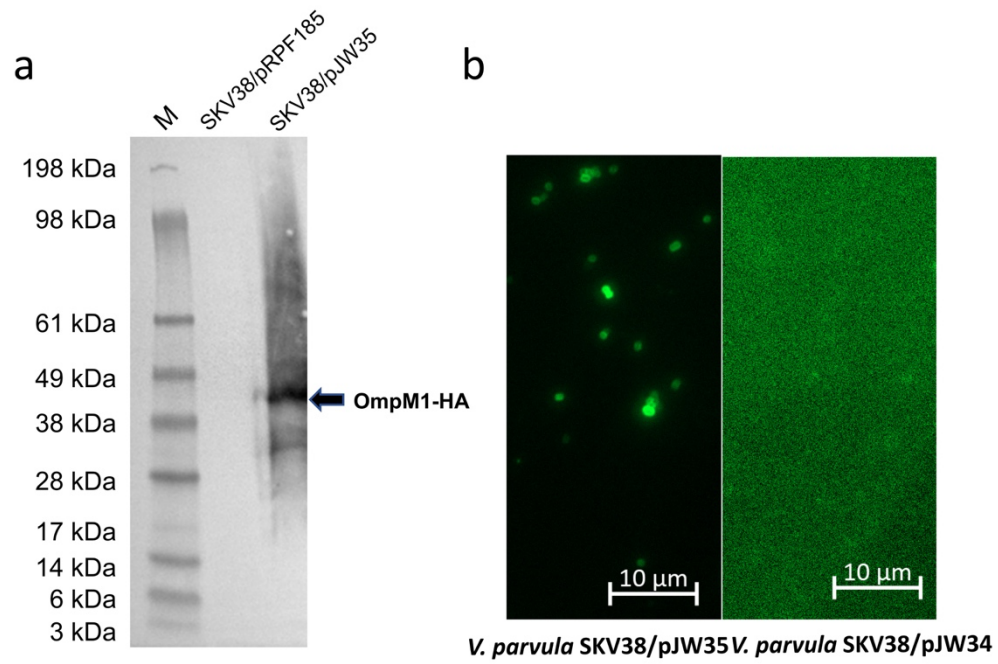


Extended Data Figure 3. The drastic phenotype of the $\Delta ompM1-3$ mutant cannot be complemented by expressing *in trans* OmpM4 or OmpA. In (a) the $\Delta ompM1-3$ was transformed with a plasmid expressing either native (pJW63) or HA-tagged (pJW62) OmpM4 from an aTc inducible promoter. In (b) the $\Delta ompM1-3$ was transformed with a plasmid expressing either native (pJW65) or HA-tagged (pJW66) OmpA from an aTc inducible promoter. Both OmpM4-HA and OmpA-HA were readily detected by western blot using an anti-HA primary antibody coupled to horse radish peroxidase when aTc was added at 250 $\mu\text{g}/\text{l}$ (left panels). However, the strong phenotype of the $\Delta ompM1-3$ was not complemented by expressing either native or HA-tagged version of OmpM4, as well as native or HA-tagged version of OmpA, as shown on the right

panels following FM 4-64 epifluorescence. Scale bars represent 5 μm . The samples presented are representative of multiple ($n>10$) experiments.

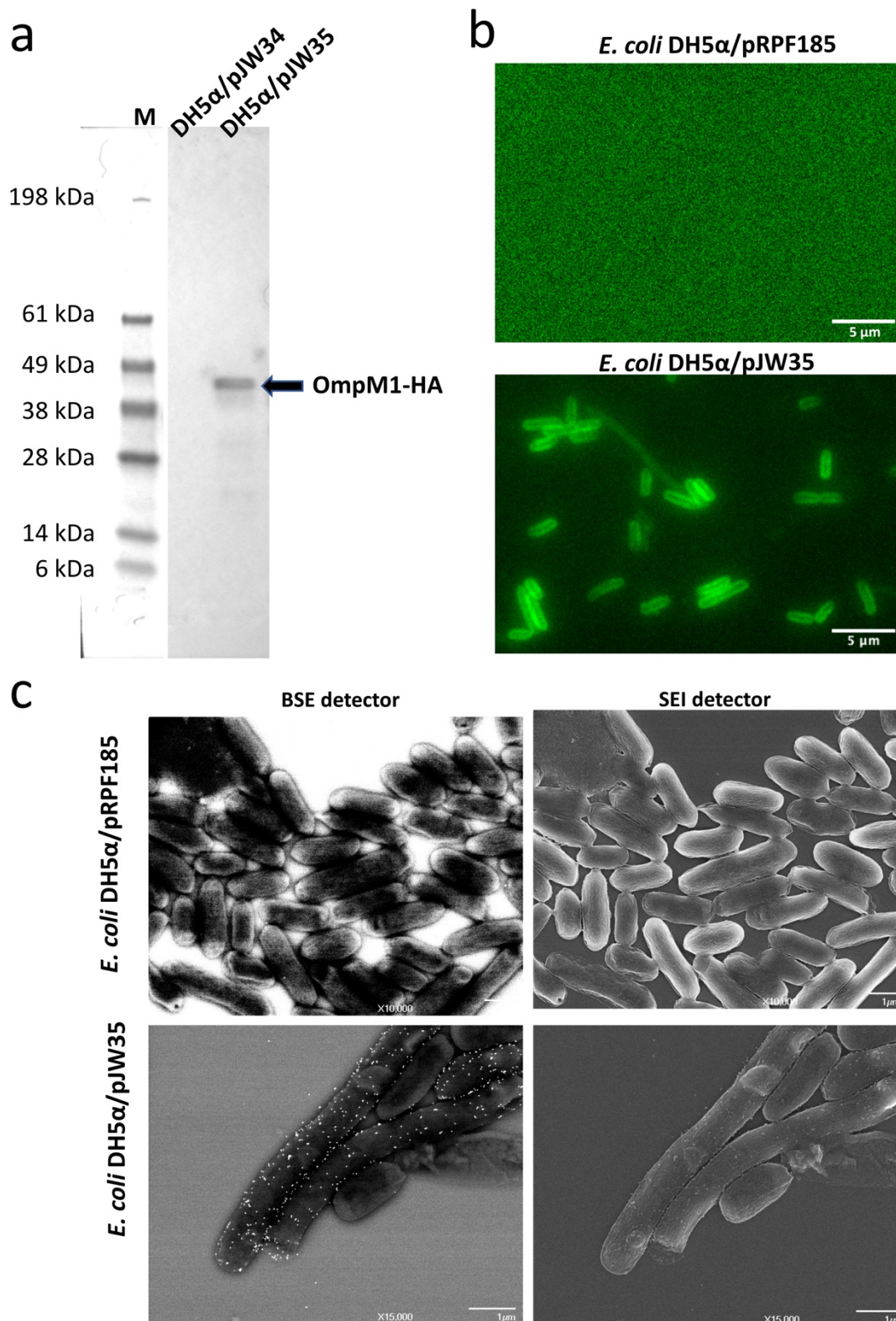


Extended Data Figure 4. Detailed characterization of the strong phenotype of the $\Delta ompM1-3$ mutant using cryoelectron tomography. Cells of the $\Delta ompM1-3$ mutant were grown for 48h in SK medium before being prepared, deposited and observed using a 300kV Titan Krios (Thermo Fisher Scientific) transmission electron microscope. Different slices of cryoelectron tomography of different positions of a mesh grid containing the $\Delta ompM1-3$ mutant are shown. Scale bars represent $0.5 \mu\text{M}$, blue arrows OM, red arrows peptidoglycan, green arrows IM, grey arrows fimbriae, yellow asterisks indicate empty vesicles. The CryoEM acquisition was performed twice, but the phenotype of the presented samples, as assessed by conventional fluorescence microscopy, is representative of multiple ($n > 20$) experiments.



Extended Data Figure 5. OmpM1 is located in the outer membrane of *V. parvula*. Comparison of WT SKV38 strain of *V. parvula* containing pRPF185 (empty vector),

pJW34, a vector expressing untagged OmpM1, and pJW35, a vector expressing HA-tagged OmpM1 both under the control of *tet* promoter. All cultures were induced overnight with 250 $\mu\text{g}/\text{l}$ anhydrotetracycline. In (a), we used an anti HA primary and antibodies coupled to horse radish peroxidase (HRP) to detect the expression of OmpM1-HA (arrow) from pJW35 by Western blot. M corresponds to SeeBlue Plus Prestained Protein Standard (Invitrogen). In (b), we performed immunofluorescence microscopy of WT cells expressing either OmpM1-HA (pJW35) or native OmpM1 (pJW34) using an anti-HA antibody coupled to fluorescein. Cells were non-permeabilized. While native OmpM1 was not detectable, OmpM1-HA that contains the HA tag in one of the predicted outer loops of its beta-barrel could be detected as all around the cell, confirming that it located in the outer membrane and is surface exposed. Surface exposition of tagged OmpM1 expressed from pJW35 was confirmed using Scanning Electron Microscopy in (c). We used anti-HA primary antibodies and secondary antibodies coupled to 20 nm gold particles on non-permeabilized cells. Images were obtained using a JEOL JSM 6700F field emission scanning electron microscope and with a backscattered electrons detector (BSE) to detect the gold labelling and with a secondary electron detector (SEI) to image the surface of the sample. The acquisitions were performed once.



vector expressing HA-tagged OmpM1 both under the control of *tet* promoter. All cultures were induced overnight with 250 $\mu\text{g}/\text{l}$ anhydrotetracycline. In (a), we used anti-HA antibodies coupled to HRP to detect, in *E. coli*, the expression of OmpM1-HA (arrow) from pJW35 by Western blot, while the non-tagged native OmpM1 expressed from pJW34 could not be detected. M corresponds to SeeBlue Plus Prestained Protein Standard (Invitrogen). In (b), we performed immunofluorescence microscopy of *E. coli* cells expressing no OmpM1 (empty vector pRPF185) or OmpM1-HA (pJW35) using an anti-HA antibody couple to fluorescein. *E. coli* cells were non-permeabilized. OmpM1-HA that contains the HA tag in one of the predicted outer loops of its beta-barrel could be detected as all around *E. coli* cells, confirming that it located in the outer membrane and is surface exposed also in this bacterium, therefore suggesting that it could be transported and inserted in the outer membrane of a classical diderm bacterium. Surface exposition of tagged OmpM1 expressed from pJW35 in *E. coli* was confirmed using Scanning Electron Microscopy in (c). We used anti-HA primary antibodies and secondary antibodies coupled to 20 nm gold particles on non-permeabilized cells. Images were obtained using a JEOL JSM 6700F field emission scanning electron microscope and with a backscattered electrons detector (BSE) to detect the gold labelling and with a secondary electron detector (SEI) to image the surface of the sample. The acquisitions were performed once.

Substance	WT	$\Delta ompM1-3$	$\Delta ompM4$	$\Delta ompA$	$\Delta ompM1-4$	$\Delta ompA$ $\Delta ompM1-4$	WT pRPF185 + ATc	$\Delta ompM1-3$ pRPF185 + ATc	$\Delta ompM1-3$ pJW34 + ATc	$\Delta ompM1-3$ pJW35 + ATc
Sodium deoxycholate	300 mg/l	5 mg/l	300 mg/l	300 mg/l	5 mg/l	<0.6 mg/l	300 mg/l	9 mg/l	150 mg/l	300 mg/l
EDTA	2500 μ M	156 μ M	2500 μ M	2500 μ M	156 μ M	<5 μ M	2500 μ M	313 μ M	1250 μ M	2500 μ M
SDS	100 mg/l	3 mg/l	100 mg/l	100 mg/l	3 mg/l	<0.2 mg/l	50 mg/l	3 mg/l	25 mg/l	50 mg/l
Vancomycin	>1000 mg/l	31 mg/l	>1000 mg/l	> 1000 mg/l	31 mg/l	<1 mg/l	500 mg/l	16 mg/l	63 mg/l	250 mg/l

Extended Data Table 1. Minimum inhibitory concentrations (MIC) of outer membrane stress inducing molecules on the five mutant strains with respect to the WT. The last four columns correspond to the complementation assay of the $\Delta ompM1-3$ mutant. pRPF185 – empty vector. pJW34 – vector expressing native OmpM1 under the control of *tet* promoter. pJW35 – vector expressing a HA-tagged version of OmpM1 under the control of *tet* promoter. +ATc – culture realized in presence of 250 μ g/l of anhydrotetracycline under chloramphenicol (25 mg/l) selection. The data presented in the table are a result of a duplicate.